

Test: A Software Signal Simulation of Low Earth Orbit Satellites for Investigative Analysis

by

Samuel McDougal

A thesis submitted to the Graduate Faculty of
Auburn University
in partial fulfillment of the
requirements for the Degree of
Master of Science

Auburn, Alabama
Sometime Spring 2023

Keywords: LEO Satellites, USRP, Navigation, Signals of Opportunity

Copyright 2023 by Samuel McDougal

Approved by

Scott Martin
David Bevly
Brendon Allen

Abstract

Place the text of the abstract here. Headings come automatically.

Acknowledgments

acknowledgments

Table of Contents

Abstract	ii
Acknowledgments	iii
1 Introduction	1
1.1 Motivation	1
1.2 Prior Work	1
1.3 Contributions	3
1.4 Thesis Outline	3
2 Background	4
2.1 Satellite Based Navigation	4
2.2 Satellite Orbit Zones	5
2.3 Low Earth Orbit Satellites	7
2.3.1 Current LEO Constellations	8
2.4 Channel Access Methods	8
2.4.1 Time Division Multiple Access	9
2.4.2 Code Division Multiple Access	10
2.4.3 Frequency Division Multiple Access	10
2.5 Modulation	10
2.5.1 Binary Phase Shift Keying	11
2.5.2 Quadrature Phase Shift Keying	12

3	Simulation Tool	13
3.1	Simulator Overview	13
3.2	Simulation Settings	14
3.3	Measurement Simulation	15
3.3.1	Introduction	15
3.3.2	Satellite Propagation	17
3.3.3	Error Generation	22
3.3.4	Measurement Calculations	24
3.4	Signal Simulation	27
3.4.1	Introduction	27
3.4.2	Initial Calculations	28
3.4.3	Data Message Generation	29
3.4.4	Signal Generation	30
3.4.5	Final Outputs	32
3.5	Receiver	32
4	Testing Setup and Positioning Techniques	36
4.1	Doppler Based Positioning	36
4.2	Pseudorange Based Positioning	39
4.3	Testing Setup	41
5	Results	43
5.1	Static Clean Data	43
5.1.1	Doppler Positioning	44
5.1.2	Pseudorange Based Positioning	45
5.2	Static Clean Data Played Through USRP	47
5.2.1	Doppler Positioning	48

5.2.2	Pseudorange Based Positioning	49
5.3	Static Noisy Data	52
5.3.1	Doppler Positioning	53
5.3.2	Pseudorange Based Positioning	54
5.4	Static Augmented Satellites	57
5.4.1	Doppler Positioning	57
5.4.2	Pseudorange Based Positioning	59
5.5	Dynamic Clean Data	62
6	Conclusions and Future Work	65
6.1	Summary	65
6.2	Conclusions	66
6.3	Future Work	67
	Bibliography	68
	Appendices	71

List of Figures

2.1	Visual Depiction of Trilateration	5
2.2	Visual Representation Orbit Zones	6
2.3	Visual Representation of TDMA Signal	9
2.4	Amplitude Shift Keying Visualization [1]	11
2.5	Frequency Shift Keying Visualization [2]	11
2.6	Binary Phase Shift Keying Visualization [3]	12
2.7	Quadrature Phase Shift Keying Visualization [3]	12
3.1	Overall Simulation Diagram	13
3.2	Measurement Generation Block Diagram	16
3.3	Propagated Satellites from SGP4	21
3.4	Signal Simulation Block Diagram	27
3.5	Signal Generation Block Diagram	31
5.1	Position Estimate from Batched Doppler Measurements	44
5.2	RMS Error of Batched Doppler Estimates	45
5.3	PDOP of Batched Doppler Estimates	46
5.4	Position Estimate from Pseudoranges	46
5.5	RMS Error from Pseudoranges	47
5.6	PDOP from Pseudoranges	48
5.7	USRP Doppler Positioning Estimate	49
5.8	RMS Error of Doppler Positioning Estimate	50
5.9	PDOP from Doppler Positioning Estimate	50

5.10	USRP Pseurorange Positioning Estimate	51
5.11	RMS Error USRP Pseurorange Positioning Estimate	51
5.12	USRP Pseurorange Positioning Estimate PDOP	52
5.13	Noisy Doppler Positioning Estimate	53
5.14	RMS Error Noisy Doppler Positioning Estimate	54
5.15	Noisy Doppler Positioning PDOP	55
5.16	Noisy Pseudorange Positioning Estimate	55
5.17	RMS Error Noisy Pseudorange Positioning Estimate	56
5.18	PDOP Dirty Pseudorange Positioning Estimate	56
5.19	Generated Augmented Satellite Constellation	57
5.20	Skyplot of Augmented Constellation	58
5.21	Doppler Position Estimates of Augmented Satellites	58
5.22	RMS Error Doppler Position Estimates of Augmented Satellites	59
5.23	PDOP of Doppler Position Estimates of Augmented Satellites	60
5.24	Pseudorange Position Estimates of Augmented Satellites	60
5.25	RMS Error of Pseudorange Position Estimates of Augmented Satellites	61
5.26	PDOP of Pseudorange Position Estimates of Augmented Satellites	61
5.27	Path Driven for Dynamic Data	62
5.28	Generated Dynamic Doppler Measurements	63
5.29	Jackson Labs Doppler Measurements	64

List of Tables

3.1	Satellite Position and Velocity Data Message	30
3.2	COE Data Message	30

Chapter 1

Introduction

1.1 Motivation

Low Earth orbit (LEO) satellites for navigation have gained interest as an alternative source of position, navigation and timing (PNT) to GNSS due to GNSS being susceptible to interferences such as jamming, spoofing, and multipath. Many current LEO satellites are not designed for navigation, however their signals have been exploited for opportunistic navigation. Many of these constellations have data messages that are unknown to the user which makes receiver design difficult. While there are a few high fidelity LEO simulators on the market, they can be expensive. These tools allow for testing of signal types before satellites are launched and signals can be replicated with prior knowledge of the signal. The development of a signal simulation tool that allows for testing of different signal types, satellite constellations, and receiver patterns is a necessary tool for developing software and hardware receivers for LEO satellites.

1.2 Prior Work

There are recent studies in positioning techniques with the growing interest in finding navigation possibilities with LEO satellites. Currently, global navigation satellite systems (GNSSs) are an integral part of modern society. Whether it is directions to the grocery store, land surveying, or autonomous vehicles, the knowledge of where something is and where it is supposed to

go is important. Current GNSSs, such as Global Positioning System (GPS), use radio frequencies (RF) to determine position and velocity solutions. Methods for calculating positions and velocities from GPS satellites can be found in [4].

The flexibility of a simulation tool is crucial. It saves time, money, and resources when testing different scenarios. One of the biggest advantages to this simulation tool is the ability to interchange different pieces quickly and efficiently. Whether it is the constellation type, data message, or signal structure, changes can be made easily to accommodate varying test plans. Current navigation simulation tools are mainly focused on GNSSs such as [5] and [6]. One source, [7] designs a signal simulation tool for “Rapid Testing of Interference Mitigation Techniques” for GPS. In his thesis, Powell outlines structures for creating a low cost signal simulation tool that can be used to test different scenarios. He begins by generating a file of simulation settings. This is followed by a scenario simulation where satellites are propagated, measurements are generated, and the navigation message populated. Next the signal is generated for the satellites in view and the data is stored in a bin file. GNSS signal simulators can also be used to test software defined receivers (SDRs). Powell validates his simulation by comparing the generated signal performance to the performance of a hardware gps receiver and examining the position, velocity, carrier to noise ratio, and Doppler frequencies. Powell found that the simulator described in his thesis was capable of producing realistic single and multi antenna signals.

One of the main areas of research for LEO satellites is using the Doppler frequency measurements from the LEO satellites in order to gain a navigation solution [8] [9]. Doppler positioning has been used in GNSS [10], and was even the precursor to GPS [11]. The Transit satellite system was initially used for US naval ships to gain a rough position. In [12], Thompson uses a double differenced Doppler technique to position a moving rover with LEO satellites using angle of arrival (AOA) estimates to remove the need of satellite state knowledge. The Argos satellite system uses Doppler measurements for animal tracking [13]

Another area of research with LEO satellites is to use their measurements and colaberate with IMUs for opportunistic navigation[14] and [15]. In [16], the Orbcomm constellation is used to to aid an inertial navigation system (INS) in a tightly-coupled fashion. Here they used

the LEO satellite Doppler measurements and TLE files to estimate the position of a moving UAV without GNSS signals. For the experiment, the UAV was without GPS and had 2 Orbcomm satellites. They claim that this navigation framework lowered the UAV final position error by 72 percent when compared to solely using the IMU.

One possibility is to deploy a new constellation in LEO specifically for navigation [17].

A LEO satellite signal simulator can be useful for testing different signal types, constellation geometries, and possible errors. The results of a simulation are only as good as the simulator itself. While high end signal simulators exist, they can be expensive and require technical prowess to operate. A low cost version can be valuable and still operate at a high level of fidelity with more ease of use.

1.3 Contributions

This thesis will describe the process of designing a modular simulation tool for LEO satellites. The versatility of the simulator allows the user to test different scenarios. The contributions from this thesis are listed below:

- Description of LEO satellite signal simulation tool that generates realistic IQ signals to be used for current and emerging constellations
- Investigation of USRP playback and record to introduce hardware errors
- Examine possible positioning techniques for TDMA signals

1.4 Thesis Outline

In Chapter 2, the background of satellite orbits, signal types, and modulation types are discussed. In Chapter 3, the simulation tool is described in detail. Chapter 4 dives into the simulation and testing configurations used for this thesis. The results from the testing configurations are discussed in Chapter 5. Conclusions and future work are discussed in Chapter 6 followed by a list of references and an Appendix.

Chapter 2

Background

2.1 Satellite Based Navigation

Satellite navigation employs trilateration as a way to solve the age old problem of determining where ones self is on planet Earth. Trilateration is the process of using ranges to determine unknown locations of things. In a 2-dimentional example, three transmitters produce circles with radius r . With knowledge of the location of the transmitters, the ranges can be used to calculate a circle around the transmitter. The intersection point of all three circles will enclose the positioning result. This can be seen in figure 2.1.

The process of trilateration with satellites is the same except in 3-dimensional space. In the case of GPS, the satellites are the transmitters. Satellites make excellent transmitters in this case because of their ability to cover large areas continuously. An important point to mention is that in the previous example it is assumed that the satellite and receiver are tied to the same clock. This means that the user has a perfect known time of the transmission of the signal from the satellite and perfect knowledge of the time of reception. However, this is not the case in real world examples. In fact, each satellite is tied to its own clock while each receiver is also tied to a separate clock. This offset in time can cause very large errors in positioning. To account for this, GPS ground stations survey and monitor the status of the satellite clocks to ensure maximum clock accuracy. While this takes care of the satellite part of the clock issue, the receiver clock still contains error. This error can be estimated along with the receiver states with the addition of a fourth measurement. With four unknown variables (receiver position x , y , z , and clock bias b), four measurements must be available in order to estimate the unknowns.

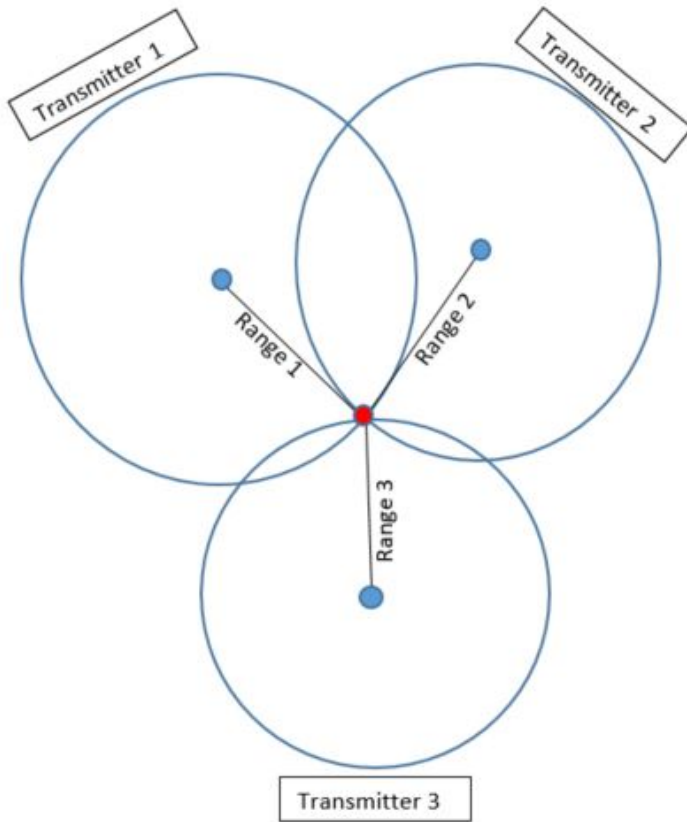


Figure 2.1: Visual Depiction of Trilateration

Satellites use radio frequencies (RF) to transmit information to users on the surface of the Earth. These RF signals have encoded data called navigation messages that users can receive and unpack with specialized RF receivers. The navigation message can contain information such as satellite positions and velocities, clock corrections, and orbital parameters. These parameters are used for obtaining the precise location of satellites to obtain ranges that is used for solving the positioning problem.

2.2 Satellite Orbit Zones

With regard to space vehicles, there are three main orbital zones. These zones are low Earth orbit (LEO), medium Earth orbit (MEO), and geosynchronous Earth orbit (GEO). These zones are differentiated by the altitude of the orbit above the surface of the Earth. Due to the nature of the orbits, the satellites in these orbital zones have varying mission types. Figure 2.2 gives a reference to each of the orbital zones.

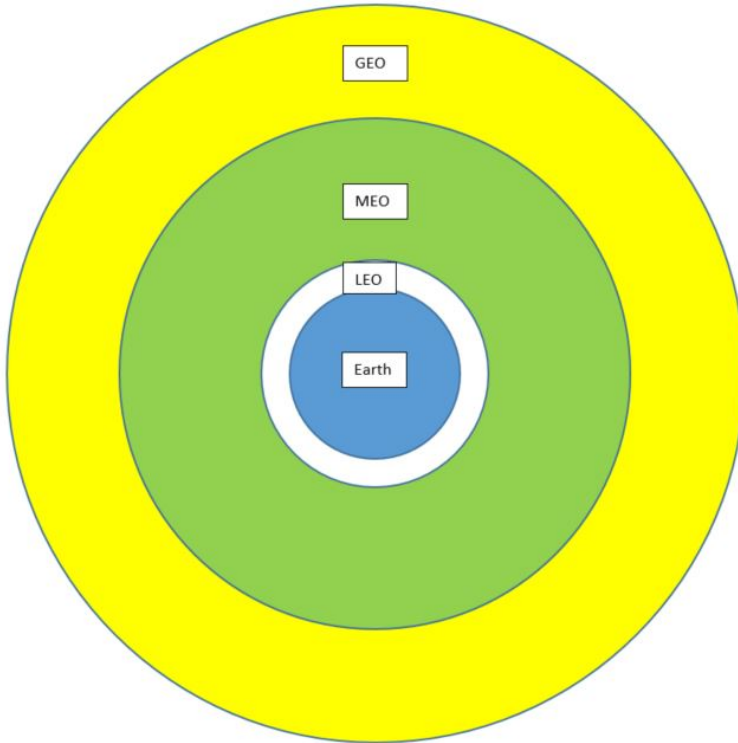


Figure 2.2: Visual Representation Orbit Zones

The furthest of the orbit zones is GEO. These satellites have an orbit altitude of 35,786 kilometers. Geosynchronous orbits are positioned at this precise altitude to allow the satellite orbit period to equal the same time as the rotation of the Earth for one day. The length of the orbit lasts one sidereal day. To an observer on Earth, the satellite would appear to stay in the same place throughout the course of its life. Another form of geosynchronous orbit is the geostationary orbit. Geostationary orbits are geosynchronous orbits specifically located at the Earth's equator and have a near zero inclination angle. GEO satellites are stationed where they are due to their specific mission type. One of the best attributes a GEO satellites has is a large footprint. The large footprint, along with the twenty four hour coverage, means these satellites are great for Earth observation. This also means that fewer satellites are required to be in orbit for full Earth coverage. Many of the current GEO satellites are used for weather, climate surveying, and oceanic observations [18]. The Geostationary Operational Environmental Satellites (GOES) are the current Earth observation satellites operated by NASA and NOAA [19]. GEO satellites are not conducive for navigation. This is due to the nature of the orbit. Since the orbit is so high, gaining a precise navigation message can be difficult due to loss of

signal power and the amount of time it takes for the signal to reach Earth. Another issue with GEO satellites is the cost of launching these satellites. Launching satellites into GEO can carry a much higher price than satellites in LEO or MEO. These points were taken into consideration when GPS was first being thought about. (Maybe include an image of GEO coverage).

MEO is an orbital zone between LEO and GEO. MEO satellites have orbit altitudes between 2,000 kilometers and 35,000 kilometers. The orbit period for most MEO satellites is between 10 hours and 15 hours. Most of the satellites in MEO are navigation satellites. These constellations include GPS (USA), Galileo(European), GLONASS (Russia), and BieDou (China). Each country with GNSSs has designed them specifically for their own use. For example, GLONASS has an orbit altitude of 19,000 kilometers with satellites at specific inclination angles in order for the satellites to spend more time in view over Russia [20]. GPS occupies MEO for many reasons, one being the number of satellites needed for global coverage. While more satellites are needed in MEO for global coverage than GEO, fewer are required than in LEO. GPS satellites have an orbit period just under 12 hours. With the orbit altitude and orbit period, 24 satellites are needed for global coverage in order to have at least 4 satellites in view to gain a positioning solution. However, with an orbit period of 12 hours, the observed Doppler frequencies of the satellites are low and can lead to poor velocity estimates. Next, LEO satellites are discussed.

2.3 Low Earth Orbit Satellites

LEO satellites are different than the previously mentioned zones. LEO satellites have orbits from 300 kilometers to 1500 kilometers. With this altitude, the orbit periods for LEO satellites tend to be 60 to 90 minutes, however the amount of time that a satellite may be in view is lower. This poses issues in terms of global coverage. Satellite constellations with orbit periods on this time scale require far more satellites for full global coverage, and even more satellites for a possible navigation constellation. Reid et al says that it would take nearly 300 LEO satellites in order to provide global coverage [17]. Current LEO constellations, such as Iridium and Orbcomm, are designed for communications. The Iridium constellation uses global coverage for satellite phones, where the Orbcomm constellation uses “LEO satellites to provide

worldwide geographic coverage for sending and receiving alphanumeric packages,” [21]. The data messages on these satellites are unknown as they are proprietary to the companies who sent them into space. This makes it difficult to design receivers and evaluate the navigation performance of these signals. However, a customized navigation message can be put on a similar signal.

2.3.1 Current LEO Constellations

Current LEO constellations were not designed for navigation, specifically. Most are used for satellite communications, internet, and Earth observations. Some of the major constellations in LEO are Iridium/IridiumNEXT, Orbcomm, and Starlink. The IridiumNEXT [22], which will be referred to as Iridium, is a telecommunications satellite network that comprises of 66 active satellites and 9 in-orbit spares. The 66 active satellites are grouped into 6 orbital planes with 11 satellites in each plane. These satellites are in near polar orbits which means the coverage at the poles is very high, however coverage at the equator is low. The main mission for Iridium is to provide telecommunications with sat-phones. Orbcomm is similar to Iridium as it is a satellite communications constellation, however the physical constellation is different. Orbcomm has 48 satellites with varying inclination angles. The Starlink constellation is a satellite broadband internet provider [23]. This constellation utilizes LEO orbit in an effort to reduce latency with internet signals. Instead of using typical terrestrial based techniques for internet providing, satellites are used to give coverage in places where internet may not be readily available. However to accomplish this goal, a massive constellation of satellites must be deployed. Currently, there are nearly 3,600 Starlink satellites in LEO with more planned for launch. All of these constellations have one thing in common. The original purpose of the mission was not for navigation.

2.4 Channel Access Methods

Channel access methods are ways of communicating through mediums between multiple devices. Channel access methods allow users to send information back and forth between terminals. Channel access methods are used to manage telecommunications and wireless traffic. As

there are multiple users trying to use or access the same information or services, channel access methods are used to differentiate between the users and the information being passed through the mediums. Three forms of channel access methods that will be examined are time division multiple access (TDMA), code division multiple access (CDMA), and frequency division multiple access (FDMA).

2.4.1 Time Division Multiple Access

Time division multiple access signals use time to differentiate incoming signals. This results in the signal being burst-like in nature and non-continuous between received signals. The carrier frequency, however, can remain the same across all users. TDMA signals are typically used by telecommunication satellites such as Iridium. These signals are ideal for communications because as the users are separated in time, the possibility of data interference between users is low. A visual representation of a TDMA signal can be seen in figure 2.3. The burst nature

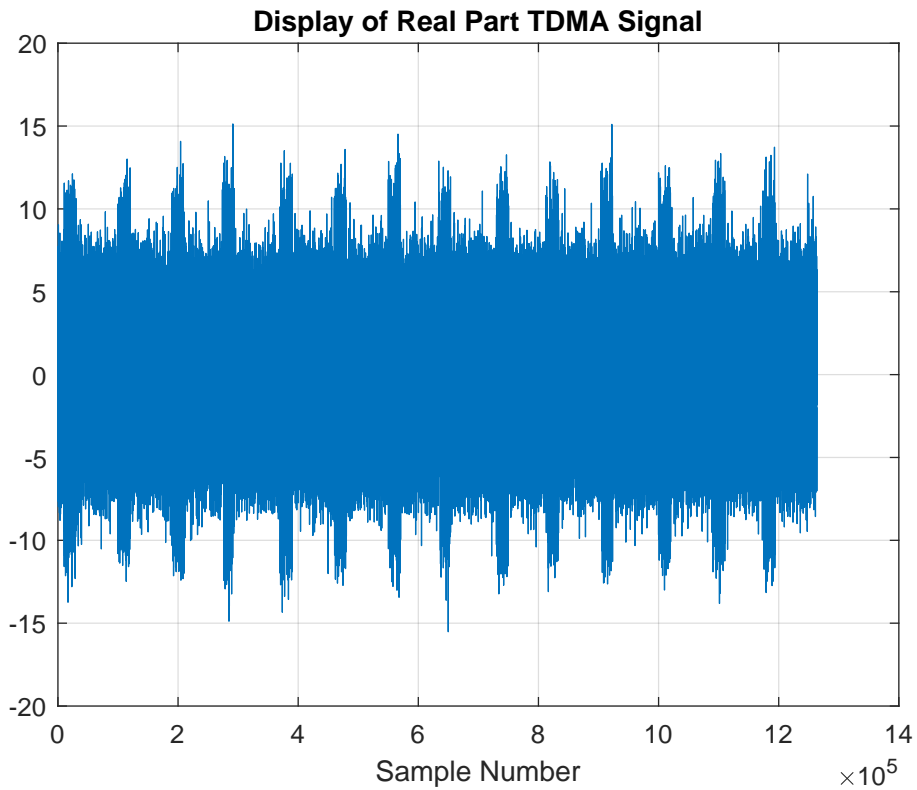


Figure 2.3: Visual Representation of TDMA Signal

of the signal can be seen in this image. The large bulk of the signal is noise, and the parts

extending out of the noise are the the bursts. This shows the separation of the signal accross time.

2.4.2 Code Division Multiple Access

Similar to TDMA, CDMA signals are broadcast at a single carrier frequency. However unlike TDMA, CDMA signals use deterministic binary sequence codes to differentiate signals. In the case of satellites, each satellite is given its own pseudo-random noise (PRN) sequence. These codes are designed specifically to have very low cross correlation in order to eliminate errors and deciphur different satellite's signals in the same frequency band. Cross correlation is a measure of similarity between two or more sequences. They also employ a high level of autocorrelation which is important for signal tracking [24]. Two notable GNSSs that employ CDMA signals are GPS and Galileo.

2.4.3 Frequency Division Multiple Access

Similar to CDMA, FDMA signals are continuous. However, these signals are not transmitted at the same carrier frequency. FDMA signals use different freqency bands to transmit data and information. For example, FM radio uses this technique to differentiate between radio channels such as sports talk radio and the local country music station. Similar to the radio in a car, some satellite constellations use the same idea, except each satellite transmits at a specific frrequency band. For example, GLONASS uses FDMA signals for their satellites but also use a PRN code. Unlike GPS, however, they all transmit the same PRN sequence [25].

2.5 Modulation

In the world of satellite navigation and telecommunications, the term modulation refers to the process of incorporating data onto a carrier wave. This data is represented in binary form through 1's and 0's. When a signal is generated, these ones and zeros are converted into 1's and -1's for the purpose of signal modulation. Three forms of modulation include amplitude shift keying (ASK), frequency shift keying (FSK), and phase shift keying (PSK). ASK is the process of changing the amplitude of the sine wave to represent ones and zeros of binary data,

FSK is the process of changing the frequency of the sine wave to represent ones and zeros of binary data, and PSK changes the phase of the signal to incorporate the data. ASK and FSK are shown in figure 2.4 and 2.5 respectively.

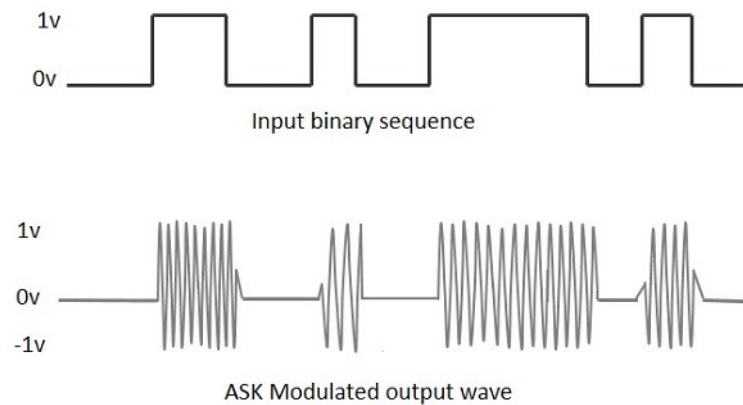


Figure 2.4: Amplitude Shift Keying Visualization [1]

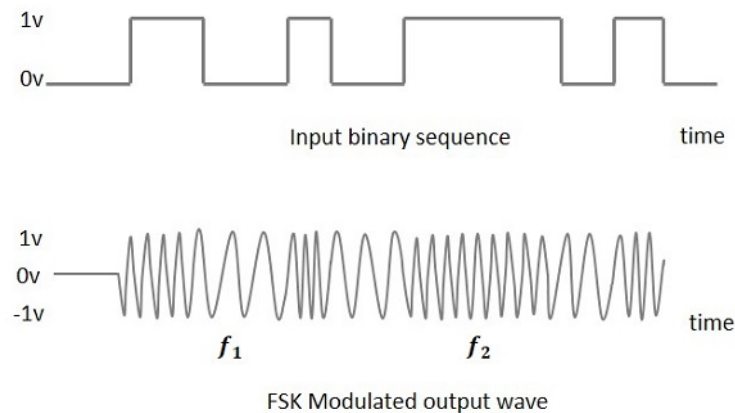


Figure 2.5: Frequency Shift Keying Visualization [2]

Two forms of PSK are binary phase shift keying (BPSK) and quadrature phase shift keying (QPSK) and will be discussed below.

2.5.1 Binary Phase Shift Keying

BPSK is accomplished by shifting the phase of the signal by 180 degrees depending on the sign of the data bit. For example, when the sign of the data bit in the message changes, the phase of the signal flips by 180 degrees. By doing so, only one bit can be modulated per symbol. GPS

uses BPSK modulation for its CA codes, navigation data, and P(Y) codes (encrypted message). BPSK is used due to its resilience to bit error rate. A visual depiction of the BPSK signal can be seen in figure 2.6. In the figure, the phase change of the signal by 180 degrees can be seen at the change of each data bit.

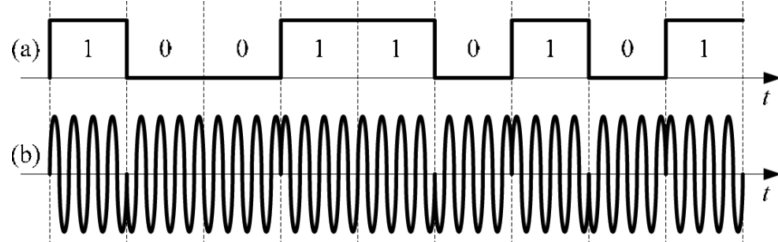


Figure 2.6: Binary Phase Shift Keying Visualization [3]

2.5.2 Quadrature Phase Shift Keying

QPSK modulation uses 4 possible phases of the signal to modulate the data onto the carrier wave. The phase possibilities are 90 degree offsets. With this, two bits are transmitted in one symbol. This allows for faster data rates of the signal. Figure 2.7 shows a visual example of QPSK modulation.

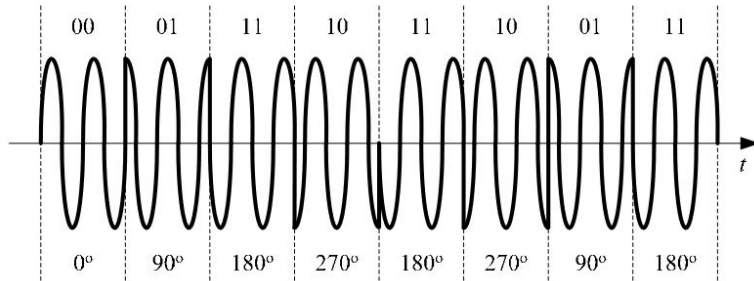


Figure 2.7: Quadrature Phase Shift Keying Visualization [3]

Chapter 3

Simulation Tool

In this section, the function and versatility of the simulator will be described.

3.1 Simulator Overview

The overall structure of the simulation is shown in figure 3.1.

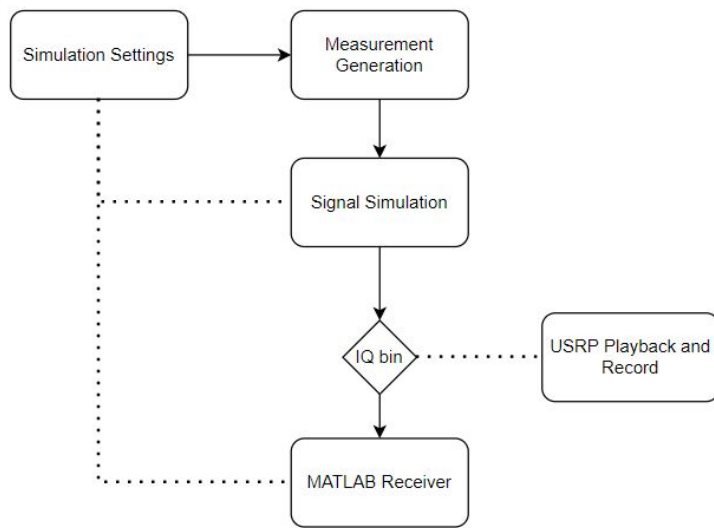


Figure 3.1: Overall Simulation Diagram

The simulation begins with the simulation settings file. This is a configuration file where all of the settings will be declared. This includes, but is not limited to, the satellite trajectories, signal power, and simulation length. The simulation settings file is fed into each block of the simulation tool. First, it goes into the measurement generation block. The measurement generation block is where the satellite positions and velocities are propagated, ranges and range

rates are calculated, and transmit and received times are produced. Those terms are pushed into the signal simulation. Inside the signal simulation block the signal is generated and packaged into a bin file. Finally, the bin file is sent to a receiver where it is picked up, processed, and decoded to produce measurements. The following subsections will address each part of the simulation.

3.2 Simulation Settings

The simulation settings is a configuration file where all of the constants and settings used throughout the simulation are declared. All of the settings are stored in a MATLAB structure labeled ‘settings’. A MATLAB structure is a data storing type where different variables can be tied to one overall variable. The purpose for incorporating all of the settings and variables in one script is to ensure all variables are in one place. This helps the user find a variable quickly and efficiently. It also aids the user by ensuring consistency across all parts of the simulation.

In part, the simulation settings allow this tool to be modular. The file begins with constants such as the speed of light, rotation rate of the Earth, Earth gravitational constants, and time constants. These will likely stay the same across any and all simulations. Next is the input of user time. This time is in the format of year, month, day, hour, minute, second and determines the start time of the simulation. Following the time starting point is the duration of the simulation in seconds and the measurement simulation sampling frequency in hertz. The next setting is the user position. Currently, the simulation allows for a static receiver with initial position defined in latitude, longitude, and altitude (LLA); however, the addition of a dynamic receiver can be made. Once the LLA position has been defined, the Earth centered Earth fixed (ECEF) position can be calculated. Next is the introduction of measurement error terms. The first set are weather terms for the error caused by the troposphere [4]. These inputs are temperature in Celsius and Kelvin, barometric pressure in millibars, and humidity as a percentage. This is followed by clock settings. Here the user declares what type of clock to use and whether the clock error is to be simulated, indicated by an on or off switch. The clock is modeled based on []. Next is the satellite propagation settings. This simulation uses a simplified general perturbation (SGP)

model for calculating satellite positions and velocities. Here the user will input a two line element (TLE) file name along with other information used in parsing the TLE. The propagation settings also includes a mask angle setting. The mask angle input is in degrees and allows the user to reject satellites under the specified elevation angle. After the satellite propagation settings are the signal settings. Here the user decides the carrier frequency, sampling frequency, code frequency, number of symbols in the data message, and signal type. One specific signal type is time division multiple access (TDMA). A TDMA signal uses time slots in the form of bursts to decipher different signals, whereas frequency division multiple access (FDMA) uses different frequency channels. If the declared signal type is TDMA, then the burst period will need to be calculated. This is followed by the noise and signal power.

The simulation settings file is integral to this simulation tool. All other components of this simulator are dependent on it. These specific dependencies will be explained in detail in the remaining subsections.

3.3 Measurement Simulation

3.3.1 Introduction

The next block of the simulation tool is the measurement generation. The measurement generation is where satellites are propagated, ranges, range rates, and times are calculated. The purpose of this section is to have a set of truth values that will be used later in the simulation. The block diagram for the measurement generation is shown in figure 3.2.

The measurement simulation begins with the input of the simulation settings file. The following settings are the main terms used in the measurement simulation:

- User Position and Velocity
- Year, Month, Day, Hour, Minute, Second of begining of simulation
- Simulation length in seconds
- Sampling frequency of measurement simulation
- Weather settings

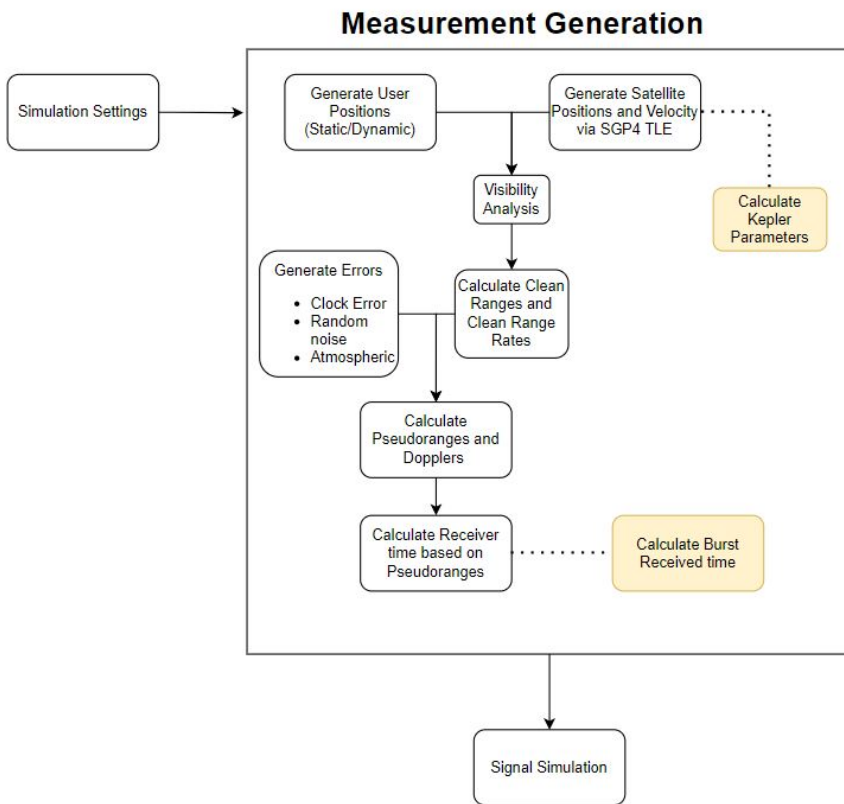


Figure 3.2: Measurement Generation Block Diagram

- Temperature in Kelvin
- Temperature in Celcius
- Barometric pressure in millibars
- Humidity as a percentage
- Clock settings
 - Receiver clock type
 - Satellite clock type
- Satellite propagation settings
 - TLE file name
 - TLE Objects
 - TLE exclude numbers

- Mask angle
- Augmented number of satellite orbital planes
- Augmented number of satellites per orbital plane
- Augmented inclination angle
- Augmented orbit altitude in meters
- Burst time (seconds)
- Toggle switches
 - Receiver type (static/dynamic)
 - Receiver clock (on/off)
 - Satellite clock (on/off)
 - Tropospheric error (on/off)
 - Satellite augmentation (on/off)
 - Additional Noise (on/off)

A breakdown of the following subsections are as follows: satellite propagation, error generation, measurement calculation, and final outputs from the measurement simulation.

3.3.2 Satellite Propagation

For this simulation tool, the simplified general perturbation (SGP4) two line element (TLE) satellite propagator is used. SGP4 is a propagation technique used to calculate positions and velocities of satellites, space debris, and orbital junk. The SGP4 TLE propagator is used to calculate near Earth objects which are classified as having orbit periods less than 225 minutes. This corresponds well for LEO satellites as the orbital period is typically between 90 and 120 minutes. The perturbations accounted for in SGP4 include solar radiation, drag, and gravitational perturbations caused by the sun and the moon. SGP4 uses TLE files as a basis of propagation. TLE files are generated for tracking space objects. These files can be found on CelesTrak.org and can be pulled in the form of a text file for current day data. TLE files are

2 lines of 69 columns with orbital and satellite data. The information inside the TLE files is shown below.

Columns Used	Term	Line Number
1	Line number	1
3-7	USSC satellite catalog number	1
8	Classification	1
10-11	Launch year	1
12-14	Launch number of year	1
15-17	Part of launch	1
19-20	Epoch year	1
21-32	Epoch day plus fractional	1
34-43	Balistic coefficient	1
45-52	Second derivative of mean motion	1
54-61	B-star drag term	1
65-68	Element Set number	1
69	Checksum	1
1	Line number	2
3-7	USSC satellite catalog number	2
9-16	Inclination angle	2
18-25	RAAN	2
27-33	Eccentricity	2
35-42	Argument of perigee	2
44-51	Mean anomaly	2
53-63	Mean motion	2
64-68	Revolution number at epoch	2
69	Checksum	2

The TLE files found on CelesTrak.org are for current space objects and satellite constellations. This simulation tool includes the option to augment the pre-existing satellite constellations with more satellites. In this case, TLEs are generated based on input values declared by the user. These terms are then used for the propagation of the satellites along with the following settings:

TLE file name This is the name of the text file with the list of TLEs for the satellite constellation being examined.

Objects The objects are the names of the satellites in the constellation. This needs to be declared for when the TLE file is parsed.

Exclude In some instances, there will be duplicates of satellites in a TLE file. These satellites need to be ignored when generating satellite data. Another instance would be when a collision has occurred with a satellite and the data tracked in the TLE is the crash object and the debris caused by it.

Simulation length This is the length of the simulation in seconds as previously mentioned.

Simulation start time The beginning time of the simulation in year, month, day, hour, minute, seconds at UTC time. Primarily the hour-minute-second because this is used for determining how far past the current epoch the satellite is being propagated at.

Measurement sampling frequency This is the rate at which measurements are generated for the simulation.

Receiver Position A vector of predetermined receiver positions in the ECEF coordinate frame. For a static receiver the vector of user positions has been generated forward for the length of the simulation at the desired sampling frequency. The vector of user positions will remain the same through the simulation as the points are not changing in the ECEF frame. For a dynamic receiver the user will input a pre-recorded or generated path that has been sampled to the sampling frequency of the simulation.

Mask angle The mask angle is declared in degrees. A mask angle is a term used to describe the range of view that a receiver will receive a signal from. For example, if a receiver was in an open area where the horizon is unobstructed, then the mask angle could be chosen to be zero degrees. However in most situations, the mask angle will be higher than zero due to unrealistic field of view of satellites at the horizon.

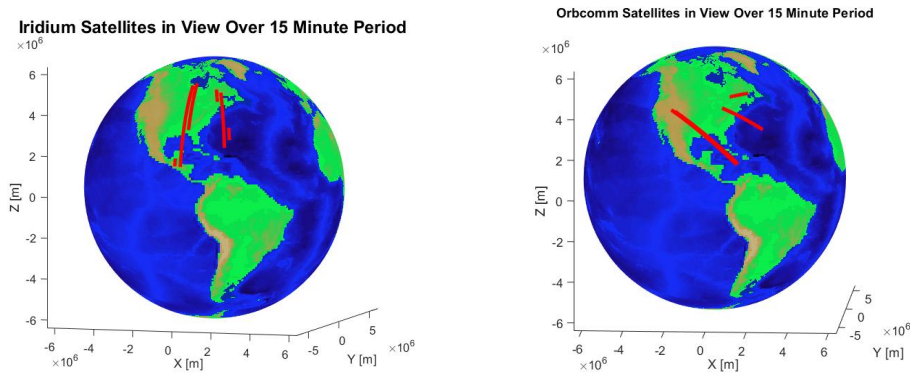
Augmentation settings As previously mentioned, the simulation tool allows the user to declare additional satellites to the current constellation being examined. The inputs from the user are number of orbital planes, number of satellites per plane, inclination angle, and orbit altitude. This feature is important for examining future constellations or investigating the performance of constellations that have not been conceived.

The SGP4 TLE propagator begins with the input of the TLE file and the simulation settings. The TLE file is parsed and a MATLAB structure is used to store each element for each individual satellite. If declared the augmented satellite orbits are generated and added to the TLE structure. An Earth orientation parameters (EOP) file is hardcoded into the simulator, however this file needs to be updated periodically manually by the user. This data can also be acquired from the Celestrak website. Time units are established and the begin time, end time, and time-step are calculated along with the time vector for the simulation. Memory is allocated for the position and velocity of each satellite in the ECEF and Earth centered inertial (ECI) coordinate frames. Next the satellites are propagated one at a time for the length of the simulation. The position and velocity vectors are put into the respective variable for ECEF and ECI. The azimuth and elevation angle are calculated for each satellite at each timestep of the simulation using the satellite positions and user positions. The elevation angles will have values $-90^\circ < El < 90^\circ$. A visibility analysis can be performed with the elevation angles. The visibility analysis takes the elevation angles and finds the satellites that are above the mask angle to eliminate them from the simulation. The output of the visibility analysis is a list of satellites and the times that they are in view. This greatly reduces the computation time for the rest of the simulation because the simulator does not calculate measurements or signals for the out of view satellites. New variables of satellite positions and velocities are generated and filled

for satellites that are in view. Mathematically this is represented in equation 3.1 where MA is the mask angle and El is the elevation angle.

$$SV_{data} = \begin{cases} Fillcell, MA < El < 90^\circ \\ NaN, MA > El \end{cases} \quad (3.1)$$

Each satellite state component (x_{sv}, y_{sv}, z_{sv} and $\dot{x}_{sv}, \dot{y}_{sv}, \dot{z}_{sv}$) for both coordinate frames are saved into individual matrices. The dimensions for each matrix is $m \times n$, where m is the length of the time vector and n is the number of satellites propagated. Figure 3.3 shows the propagated satellite orbits in view above Auburn Alabama for the Iridium and Orbcomm constellations over the duration of a 15 minute simulation.



(a) Propagated Iridium Satellites in View (b) Propagated Orbcomm Satellites in View

Figure 3.3: Propagated Satellites from SGP4

The final outputs from the satellite propagation stage are as follows:

Satellite Positions The 3-dimensional satellite position vectors in ECEF and ECI for all satellites propagated.

Satellite Velocity The 3-dimensional satellite velocity vectors in ECEF and ECI for all satellites propagated.

Elevation Angle The elevation angle of the satellites with respect to the user position.

In-view states The 3-dimensional satellite position and velocity vectors in ECEF and ECI for in-view satellites.

With the satellites propagated and a visibility analysis conducted, the next step is to calculate errors.

3.3.3 Error Generation

After the visibility analysis, errors will be generated for the satellites that are in view. Measurement errors need to be calculated for computing the received time of the signal. Two primary sources of error modeled in this thesis are clock error and tropospheric delay. As previously discussed, clocks are imperfect and have a tendency to have a bias and drift over time due to the oscillator inside of the clock. For example, satellite clocks are more accurate because they use atomic clocks where receivers typically use a crystal oscillator. The tradeoff is cost because atomic clocks are significantly more expensive than crystal oscillators. The satellite clock and receiver clock will have independent biases and drifts. The satellite is assumed to be capable of knowing and transmitting its bias and drift, while the receiver clock must be estimated by the receiver. Tropospheric delay is the error caused by gasses in the Earth's atmosphere. The atmosphere is composed of dry gasses and water vapor. These molecules have a refractive properties that effect RF signals. The input settings for these errors are as follows:

Clock Toggle There is a setting in the simulator where the user can choose to turn on or off the generated clock error. There is a switch for both the satellite clocks and the receiver clocks.

Clock Type The user will declare what type of clock to model for both the satellite and the receiver. Inside the clock error generation function, there are pre-set clocks and clock terms.

Troposphere Toggle There is a toggle switch to turn the tropospheric delay on or off.

Temperature There are two inputs for temperature. One is in Kelvin and the other is in degrees Celcius.

Atmospheric Pressure The atmospheric pressure is declared in millibars.

Humidity The humidity of the current time of simulation is input as a percentage.

The first error generated is clock error. The clock bias and clock drift are calculated for each satellite in view over the simulation based on the clock type described by the user. Next the receiver clock is modeled and the bias and drift are generated. These terms will be calculated based on [26]. As previously mentioned, this option can be turned off and the errors will be incorporated as zeros in the simulation. The current clock types in the simulator are shown in the table 3.3.3.

Oscillator	Acronym
Cesium	Cesium
Rubidium	Rubidium
Oven Controlled Crystal Oscillator	OCXO
Temperature Controlled Crystal Oscillator	TCXO

Next the tropospheric delay is calculated from the settings defined previously. The model used is found in [4]. In this thesis the tropospheric delay is modeled as a function of elevation angle with the definition of obliquity factors. This is also referred to as mapping functions. The equation for tropospheric delay is

$$\tilde{T} = \tilde{T}_{z,d} \cdot m_d(el) + \tilde{T}_{z,w} \cdot m_w(el) \quad (3.2)$$

where $\tilde{T}_{z,d}$ and $\tilde{T}_{z,w}$ are the dry and wet tropospheric zenith delay, respectively, and m_d and m_w are the mapping functions for the dry and wet components. The Saastamoinen model is used for calculating the dry tropospheric zenith delay is calculated as

$$\tilde{T}_{z,d} = 0.002277(1 + 0.0026\cos 2\phi + 0.00028H)P_0 \quad (3.3)$$

where ϕ is the latitude of the receiver, H is the height of the receiver, and P_0 is the total pressure. The wet tropospheric zenith delay is calculated as

$$\tilde{T}_{z,w} = 0.002277 \left(\frac{1255}{T_0} + 0.05 \right) e_0 \quad (3.4)$$

where T_0 is the temperature in Kelvin and e_0 is the partial pressure due to water vapor.

The mapping function for the dry delay is

$$m_d(el) = \frac{1}{\sin(el) + \frac{0.00143}{\tan(el)+0.0445}} \quad (3.5)$$

and the mapping for the wet delay is

$$m_w(el) = \frac{1}{\sin(el) + \frac{0.00035}{\tan(el)+0.017}} \quad (3.6)$$

Finally, the addition of white Gaussian noise is added for errors not modeled (i.e. Ionosphere delay, multipath, etc).

The final outputs of the error generation are as follows

Satellite Clock Error The error caused by satellite clocks. This is a MATLAB structure that is indexed for each satellite in view with fields of bias and drift. The error caused by bias and drift have units of meters and meters per second, respectively.

Receiver Clock Error The error caused by the receiver clock. The receiver clock error is saved into the same structure as the satellite clock error labeled 'ClockError'. The units for error caused by the bias and drift are also meters and meters per second, respectively.

Tropospheric Error The error caused by the troposphere. This will be a matrix of tropospheric error for each satellite in view at each time step of the simulation. The units for tropospheric error are output in meters.

3.3.4 Measurement Calculations

With the errors generated, the measurements are calculated. The measurement calculations section only has one input from the simulation settings. This input is the burst timing of the signal. The user will declare this in terms of seconds. This step needs to be included because the receive time of the signal is calculated based on the satellite burst time. This will be discussed later in the section. This subsection will give the equations used for calculating true ranges and range rates, pseudoranges and pseudorange rates, Doppler frequency, received time, and Kepler orbital parameters.

The true satellite to receiver ranges are calculated along with the range rates. Their equations are show below.

$$r = \sqrt{(x_{sv}^{(k)} - x_u)^2 + (y_{sv}^{(k)} - y_u)^2 + (z_{sv}^{(k)} - z_u)^2} \quad (3.7)$$

$$\dot{r} = (\mathbf{v}^k - \mathbf{v}_r) \cdot \mathbf{\hat{1}} \quad (3.8)$$

Having generated ranges, range rates, and errors, the receiver observed pseudorange and Doppler measurements can be calculated. The equations for pseudorange, pseudorange rate, and Doppler are equations 3.9, 3.10, and 3.11, respectively.

$$\rho^{(k)} = r^{(k)} - b_{sv} + b_r + T + \epsilon \quad (3.9)$$

$$\dot{\rho} = \dot{r} + \dot{b}_r - \dot{b}_{sv} + \epsilon \quad (3.10)$$

$$f_{Doppler}^{(k)} = \frac{\dot{\rho}}{-\lambda} \quad (3.11)$$

Where in equation 3.9, ρ is the observed pseudorange calculated from range r to the k^{th} satellite, satellite clock bias b_{sv} , receiver clock bias b_r in meters, troposphere delay T , and additional noise for errors not modeled ϵ . In Equation 3.10, \dot{r} is the calculated range rate, \dot{b}_r is the receiver clock drift, \dot{b}_{sv} is the satellite clock drift, and un-modeled errors ϵ , all with units of meters per second. In equation 3.11, $f_{Doppler}^k$ is the Doppler frequency of the k^{th} satellite, $\dot{\rho}$ is the pseudorange rate, and λ is the wavelength of the carrier. Once the pseudorange and Doppler measurements have been calculated, the observed receive time of the signal can be calculated. It is important to calculate the received time of the signal based on the pseudorange because the signal is generated at the received level. The received time is calculated as

$$t_{rx} = t_{tx} + \frac{\rho}{c} \quad (3.12)$$

where t_{tx} is the transmit time, ρ is the pseudorange calculated in equation 3.9, and c is the speed of light. For a TDMA signal, burst timing needs to be calculated. For example, if the burst timing 70 milliseconds, then a burst will at $t = 0s$, $t = 0.07s$, $t = 0.14s$ and so on. For this instance, the received time of the signal is also calculated on the burst interval using equation 3.12.

An option the user has for a data message type is Kepler orbital parameters or classical orbital elements (COE). The calculation of COE uses the ECI satellite positions and velocities calculated previously. These terms are: h magnitude of angular momentum; e eccentricity; $RAAN$ right ascension of the ascending node, i inclination angle; w argument of perigee; TA true anomaly; a semi major axis. This process is described in. [27].

The final outputs from the measurement generation are as follows:

Satellite States The positions and velocities of satellites that are in view for the duration of the simulation in meters and meters per second, respectively for both the ECEF and ECI frames.

True Range The true range of the satellite to the receiver in meters.

True Range Rate The true range rate of the satellite to the receiver in meters per second.

Pseudorange The calculated pseudoranges of the satellite to the receiver in meters

Pseudorange Rate The calculated pseudorange rate of the satellite to the receiver in meters per second.

Doppler Frequency The calculated Doppler frequency in Hz.

Transmit Time The transmit time of the satellites in seconds of simulation and in GPS time.

Received Time The received time of the signal in seconds.

COE Classical orbit elements that have been calculated for a possible data message.

3.4 Signal Simulation

3.4.1 Introduction

The signal simulation begins directly after the measurement generation and is, naturally, where the signal is created. This simulation tool is for a QPSK TDMA signal as described in section 2.5.2 and 2.4.1, respectively. Figure 3.4 gives an overview of the signal simulation. Inside the signal simulation the data message is generated and converted to binary data, received times are converted from seconds to samples, signal noise is generated, the signal is generated, separated into real and imaginary parts, interleaved, and written to a bin file. The signal output will be a file of in-phase and quadrature (IQ) data.

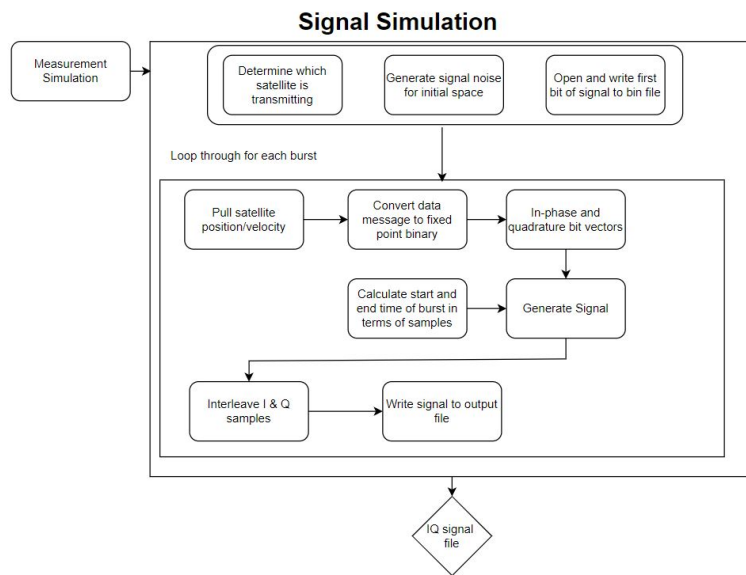


Figure 3.4: Signal Simulation Block Diagram

The main settings used for the signal simulation are as follows

- Carrier frequency in Hz
- Carrier wavelength
- Signal sampling frequency in Hz
- Code frequency
- Symbols per burst

- Code period
- Burst length in seconds
- Block size
- Signal noise power in decibels
- Signal noise power in watts
- Carrier to noise ratio
- Signal power in decibels
- Signal power in watts
- Noise toggle switch (on/off)
- Generate signal (on/off)
- Burst time in seconds

The following subsections will proceed as follows: initial calculations, data message generation, and signal generation.

3.4.2 Initial Calculations

Initial calculations that are made for the signal simulation are initial signal noise and satellite transmission determination. Since the beginning of the simulation begins the transmission of a burst and the simulation is based on what is seen by the receiver, an initial section of noise must be calculated to account for the transmission of the initial burst. Also, since only one burst occurs within the specified burst period, satellites must be chosen to transmit at specific times. The inputs for this section are as follows:

Signal Noise Toggle The signal noise toggle switch is used to turn on and off the signal noise.

Signal Noise The power of the noise floor.

Sampling Frequency The sampling frequency of the signal in Hz.

The simulation starts by determining what satellite is transmitting and stores it into an array. This process is probabilistic and one satellite in view is chosen at random to transmit. This process is performed for each burst at the start of the signal simulation. Once the burst transmission list has been determined, the first part of the signal is generated. The first part of the output file will be signal noise. The signal noise will be the length of the first transit time in terms of samples. For example, if the first transit time is 0.003009 seconds and the sampling frequency is one megahertz, the first 3009 samples will be noise. Next a bin file is generated and signal noise is written to the file.

3.4.3 Data Message Generation

The data message is a part of the signal used to gain information about the object transmitting the signal. For satellites, the data message is a package of numerical values representing the state of the satellite. This can be the satellite position and velocity, orbital elements, clock states, etc. With the calculated received times and designated satellites, the signal can be generated in blocks started by gathering the information for the data message. For this simulation, there are two options for a navigation message. The first option is to broadcast the satellite positions and velocities at the time of broadcast, or the Kepler orbit parameters at the time of transmission can be used. Next, those terms are converted into fixed point binary strings. The data bits are generated in a separate function that is specific to the data message type. The length of each word is predetermined inside the data bit generation function. The fractional length is determine based on the amount of precision the user desires. The decision to sign the word is also declared. The branch of in-phase or quadrature has also been predetermined. The outputs of the bit generation function are two row vectors of in-phase and quadrature bits. Non return to zero (NRZ) coding is used to represent the binary ones and zeros. Next, the number of samples in the signal block is determined by examining the begin time of the current burst and the begin time of the next burst. The difference in time is calculated and multiplied it by the signal sampling frequency in order to calculate the number of samples in the block. Options for the data message types can be seen in table 3.1 and table 3.2 below.

Satellite Position and Velocity ECEF			
Term	Total bits	Fractional bits	Branch
Satellite ID	8	0	Q
Satellite Pos.	32	7	Q
Satellite Vel.	32	7	Q
Transmit Time	64	0	I

Table 3.1: Satellite Position and Velocity Data Message

Kepler Elements			
Term	Total bits	Fractional bits	Branch
Sat ID	8	0	I
h	48	32	Q
e	48	57	Q
$RAAN$	48	45	Q
i	48	47	Q
w	48	47	Q
TA	48	45	Q
a	48	35	Q
Transmit time	48	17	I

Table 3.2: COE Data Message

The satellite positions and velocities mentioned in table 3.1 are for each individual cartesian component of the satellite position and velocity.

3.4.4 Signal Generation

Next is the generation of the signal shown in figure 3.5. This is where all parts of the signal are combined together and generated.

The inputs to the signal generation block are as follows:

Signal power The power of the signal.

Sampling frequency The sampling frequency of the signal in Hz.

Block size The size of the block in terms of samples.

Doppler frequency The previously calculated received Doppler frequency.

Signal noise A section of signal noise generated for the length of the burst.

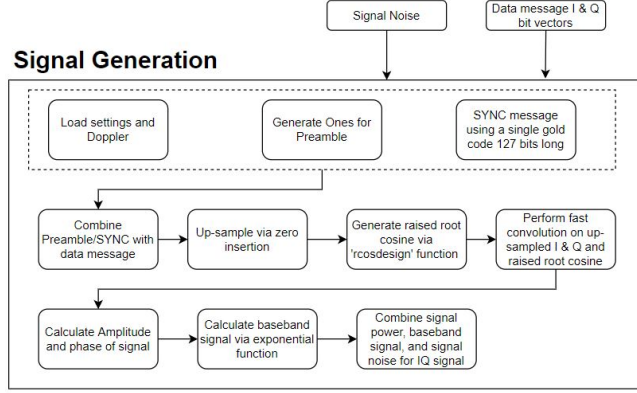


Figure 3.5: Signal Generation Block Diagram

Data message The in-phase and quadrature bit vectors of the data message.

A section of signal noise is generated for the amount of samples in the signal block. The sync message and preamble are a set of alphanumeric values that when converted to binary values have good autocorrelation properties [28]. The autocorrelation is important for the receiving and decoding of the signal and will be discussed further in this chapter. The preamble and sync messages are combined to their respective branches along with the in-phase and quadrature bit vectors to produce the full data message. If the number of bits used by the data message is lower than the number of bits in the burst, the remaining bits will be assigned random binary values. Up-sampling via zero insertion and filtering with a root-raised-cosine (RRC) pulse shaping filter is performed. The signal has to be up-sampled in order to meet the requirements set by the sampling frequency. The amplitude of the signal is calculated as equation 3.13 and the phase is calculated in equation 3.14

$$A = \sqrt{Ips^2 + Qps^2} \quad (3.13)$$

$$\theta = \tan^{-1} \frac{Qps}{Ips} \quad (3.14)$$

where Ips and Qps are the pulse shaped in-phase and quadrature branches respectively. The signal is generated through an exponential function in equation 3.15

$$Ae^{j2\pi(f_{Doppler}t+\theta)} \quad (3.15)$$

where A is the amplitude and θ is the phase. From here the declared signal power is added along side the signal noise. The output of the signal generation function is a full IQ signal with signal noise. The signal is then split into real and imaginary parts, where they are interleaved and written to the bin file. To save computational memory, the signal variables are cleared with each iteration. This process is performed for each block of signal throughout the simulation. At the end of the simulation, if there is a received time outside the bounds of the simulation time, then the simulation will end the file with signal noise.

3.4.5 Final Outputs

The final outputs of the signal simulation are as follows:

Bin file A bin file with the generated signal where the real and imaginary parts of the signal have been interleaved.

I and Q bit matrix A matrix with the in-phase and quadrature bit vectors of each burst are saved. These values are saved for analysis of bit rate error that will be observed in the results section of this thesis.

Navigation Data A matrix of navigation data which includes the satellite number, satellite states, and transmit time for each burst is saved for analytical purposes later in this thesis.

3.5 Receiver

For this thesis, a specialized receiver was designed to process and verify the signal. The receiver is based on the receiver in [29] The purpose of a receiver is to take incoming RF data and process it into observables. These observables can be used to form a positioning solution. The inputs to the receiver are as follows:

Sampling frequency The sampling frequency of the signal.

Sampling period The period of the sampling frequency.

Burst length The length of the burst in terms of samples.

Bin filename The name of the bin file generated in 3.4.4

Preamble and Sync The preamble and sync message to calculate a local replica.

Burst time The period of time between bursts.

The receiver employs a matched filter. A matched filter is a way of detecting the signal by comparing it to a local replica of some part of the signal. In order to perform a matched filter some prior knowledge of the signal must be known. In the case of this simulator the known part of the signal that remains constant across all bursts is the preamble and sync message. The preamble and sync message need to contain strong auto correlation properties in order to perform the match filtering. With a local replica of the known preamble and sync message, bursts can be detected. Before burst detection can proceed, the a coarse frequency estimate must be performed. This is because matched filters work at low frequency. As the incoming signal is pulse shaped, the bandwidth is lowered and creates a peak at the center frequency. This is used to estimate the Doppler frequency in equation 3.16.

$$f_d = \text{argmax}(R(f)) \quad (3.16)$$

Here f_d is the estimated Doppler frequency and $R(f)$ is the Fourier transform of the received signal. Next the Doppler frequency is removed by equation 3.17

$$r_{new}(t) = e^{-j2\pi f_d t} \times r(t) \quad (3.17)$$

where $r_{new}(t)$ is the new signal without the Doppler frequency and $r(t)$ is the previous raw input signal. This process is performed across the bin file until the end of the file. The output of this is an estimate of the Doppler frequency, burst location, and burst number. The burst location will be used later to calculate a pseudorange.

Next, a raised rood cosine filter is used to filter the signal to raise the signal to noise ratio which helps with signal demodulation. An approximate symbol timing is used to provide a decimation period. The decimation period allows the received signal to be resampled at one sample per symbol. This is followed by removing residual frequency and phase. This is performed through a frequency and phase discriminator. The equation for the frequency discriminator is

$$f_{remaining} = \frac{atan2(cross, dot)}{t_2 - t_1} \quad (3.18)$$

where *cross* and *dot* are

$$cross = I_1Q_2 - I_2Q_1 \quad (3.19)$$

$$dot = I_1I_2 + Q_1Q_2 \quad (3.20)$$

where I_1 and Q_1 are the sums of the first half of the tone and I_2 and Q_2 are the the sums of the second half of the tone. The remaining frequency can be wiped off by substituting f_d with $f_{remaining}$ and r with r_{new} in equation 3.17. The phase is calculated as

$$\theta = atan2(Q/I) - \frac{\pi}{4} \quad (3.21)$$

and the phase error is removed by

$$D(t) = e^{(j\theta)r(t)} \quad (3.22)$$

where $r(t)$ is the post frequency descriminated signal and $D(t)$ is the output data bits.

Once the navigation bits have been demodulated they can be parsed and converted from binary values to full numerical values. The terms and values in table 3.1 and table 3.2 are used to know what the location in the vector of bits each word occupies and how to convert back to numerical values.

The final outputs of the receiver simulation are as follows:

Decoded satellite data The decoded navigation message of satellite number, satellite position, satellite velocity, and transmit time. If the chosen output is Kepler elements, the satellite positions and velocities will already be calculated.

Estimated Doppler The estimated Doppler frequency from the receiver in Hz.

Range rate The calculated range rate from the estimated Doppler frequency.

Output bits The output bits from the navigation message are saved to compare with the generated values.

Failed burst This is a list of bursts that were observed, but the receiver failed to decode the data correctly.

Delta burst time This is the change in time from previous burst. This term will be used to calculate a pseudorange for possible positioning.

Chapter 4

Testing Setup and Positioning Techniques

This chapter will discuss positioning techniques used for validation of results in this thesis. Two specific positioning techniques are Doppler based and Pseudorange based. These techniques will be used along with the outputs of the receiver in order to gain a positioning solution.

4.1 Doppler Based Positioning

Doppler positioning is not a new technique. In fact it was used with the original TRANSIT system in the 1960's and positioning accuracy was found to be within 500 meters. Doppler shift occurs as a result of a transmitter moving relative to an observer. As the transmitter moves closer, the frequency of the signal increases as the wave is being pushed closer to the observer. The opposite is true as the transmitter moves away from the user. The basis of Doppler positioning is using the change in signal frequency to gain an understanding of the motion of the transmitter. That information along with known satellite states can be used to gain a positioning solution.

The outputs of the receiver detailed in this thesis include the satellite position vector \mathbf{r}_{sv} , the satellite velocity vector \mathbf{v}_{sv} and the received Doppler frequency $f_{Doppler}$. By rearranging 3.11, the pseudorange rate of the k^{th} satellite can be calculated in 4.1.

$$\dot{\rho}^k = f_{Doppler}^k \cdot -\lambda \quad (4.1)$$

Using 4.1 and 3.8 to rearrange 3.10, the following equation is developed.

$$\dot{\rho}^k = (\mathbf{v}^k - \mathbf{v}_u) \cdot \frac{(\mathbf{x}^k - \mathbf{x}_u)}{\|\mathbf{x}^k - \mathbf{x}_u\|} + \dot{b} + \epsilon^k \quad (4.2)$$

For a static receiver \mathbf{v}_u in equation 4.2 will be zero resulting in equation 4.3.

$$\dot{\rho}^k = \mathbf{v}^k \cdot \frac{(\mathbf{x}^k - \mathbf{x}_u)}{\|\mathbf{x}^k - \mathbf{x}_u\|} + \dot{b} + \epsilon^k \quad (4.3)$$

With knowledge of the satellite states from the decoded navigation message, the unknowns are \mathbf{x}_u and \dot{b} , where

$$\mathbf{x}_u = \begin{bmatrix} x_u \\ y_u \\ z_u \end{bmatrix}. \quad (4.4)$$

With four unknowns, at least four measurements will be needed to solve for a positioning solution. An iterative process can be used to solve for the unknowns. First, an initial estimate of the states must be made. This will be represented by

$$\hat{\mathbf{x}} = \begin{bmatrix} \hat{x}_u \\ \hat{y}_u \\ \hat{z}_u \\ \hat{b} \end{bmatrix} \quad (4.5)$$

where the \mathbf{x} is the vector of all unknown states, including the clock term. Next is a vector of pseudorange rate measurements from 4.1 taking the form

$$\dot{\rho} = \begin{bmatrix} \dot{\rho}_1 \\ \dot{\rho}_2 \\ \vdots \\ \dot{\rho}_n \end{bmatrix} \quad (4.6)$$

where n is the number of measurements being used. Next an estimate of the pseudorange rate is calculated for each satellite by combining 4.5 and 4.3 to form

$$\hat{\dot{\rho}} = \begin{bmatrix} \mathbf{v}_1 \cdot \frac{(\mathbf{x}_1 - \hat{\mathbf{x}}_u)}{\|\mathbf{x}_1 - \hat{\mathbf{x}}_u\|} + \hat{b} \\ \mathbf{v}_2 \cdot \frac{(\mathbf{x}_2 - \hat{\mathbf{x}}_u)}{\|\mathbf{x}_2 - \hat{\mathbf{x}}_u\|} + \hat{b} \\ \vdots \\ \mathbf{v}_n \cdot \frac{(\mathbf{x}_n - \hat{\mathbf{x}}_u)}{\|\mathbf{x}_n - \hat{\mathbf{x}}_u\|} + \hat{b} \end{bmatrix} \quad (4.7)$$

The measurement matrix $\mathbf{H}(\hat{\mathbf{x}})$ takes the form below where it is an $n \times 4$ matrix, where n is the number of measurements being used.

$$\mathbf{H}(\hat{\mathbf{x}}) = \begin{bmatrix} \frac{(\mathbf{x}_1 - \hat{\mathbf{x}}_u)}{\|\mathbf{x}_1 - \hat{\mathbf{x}}_u\|} \times \left(\frac{(\mathbf{x}_1 - \hat{\mathbf{x}}_u)}{\|\mathbf{x}_1 - \hat{\mathbf{x}}_u\|} \times \frac{\mathbf{v}_1}{\|\mathbf{x}_1 - \hat{\mathbf{x}}_u\|} \right) & 1 \\ \frac{(\mathbf{x}_2 - \hat{\mathbf{x}}_u)}{\|\mathbf{x}_2 - \hat{\mathbf{x}}_u\|} \times \left(\frac{(\mathbf{x}_2 - \hat{\mathbf{x}}_u)}{\|\mathbf{x}_2 - \hat{\mathbf{x}}_u\|} \times \frac{\mathbf{v}_2}{\|\mathbf{x}_2 - \hat{\mathbf{x}}_u\|} \right) & 1 \\ \vdots & \vdots \\ \frac{(\mathbf{x}_n - \hat{\mathbf{x}}_u)}{\|\mathbf{x}_n - \hat{\mathbf{x}}_u\|} \times \left(\frac{(\mathbf{x}_n - \hat{\mathbf{x}}_u)}{\|\mathbf{x}_n - \hat{\mathbf{x}}_u\|} \times \frac{\mathbf{v}_n}{\|\mathbf{x}_n - \hat{\mathbf{x}}_u\|} \right) & 1 \end{bmatrix} \quad (4.8)$$

With this form, an estimate of the position and clock drift can be calculated using an iterative process. The first step of the process is to fill in equation 4.8 with the initial guess position guess, satellite positions, satellite velocities. The next process is to calculate the pseudorange rates using 4.7. The next process is to create a delta pseudorange rate using equation 4.9.

$$\delta\dot{\rho} = \dot{\rho} - \hat{\dot{\rho}} \quad (4.9)$$

By using the delta pseudorange rate, the error of the original estimate is what is being calculated. This is calculated through least squares shown in equation 4.10.

$$\tilde{\mathbf{x}} = (\mathbf{H}^T \mathbf{H})^T \mathbf{H}^T \delta\dot{\rho} \quad (4.10)$$

The new position estimate is calculated through 4.11.

$$\hat{\mathbf{x}}_{\text{new}} = \hat{\mathbf{x}}_{\text{old}} + \tilde{\mathbf{x}} \quad (4.11)$$

This process is continued iteratively until some threshold is met. Once the threshold is met, the process is concluded and the position and clock drift are output.

This process is typically employed using four or more measurements at the same time. For this thesis, a batched technique will be used. Since the nature of the signal used in this thesis is discontinuous, only one measurement is received at each time. One way to combat this is to use batched measurements. Batching measurements means taking measurements over a select period of time and treating them as if they all have come at one time. The advantage of batching measurements is that it allows the user to have enough measurements to gain an accurate position. Typically, when batching measurements, many measurements must be used in order to gain geometric diversity apart from each other. One disadvantage of batching measurements is that it can take longer periods of time to gather enough measurements in order to gain a position estimate. Long term, the act of batching measurements is similar to averaging them all over time.

4.2 Pseudorange Based Positioning

Pseudorange based positioning is also not a new concept. Pseudoranges are used to solve the trilateration problem discussed in section 2.1. Equation 3.9 previously discussed is the pseudorange equation. It includes the true range, satellite and receiver clock errors, atmospheric errors, and unmodeled effects. Similar to the Doppler positioning in section 4.1, an iterative process is used to solve for a positioning solution. However instead of using the range rate, the pseudorange is used. There are a few modifications that need to be made to the equations used in this process, however the process of solving for the position as a whole is quite similar.

First, the burst location in 3.5 is used to generate a pseudorange. A hot start is assumed in order to gain the first range to the satellite. The burst location can be used to calculate how much the pseudorange has changed between bursts. This is modeled as

$$\rho_k(t) = \rho_k(t-1) + \frac{(bl(t) - bl(t-1))}{f_s} \cdot c \quad (4.12)$$

where bl is the burst location in terms of samples, f_s is the sampling frequency of the signal, and c is the speed of light. This is performed for each satellite that has been received.

The pseudorange model to the k^{th} satellite is

$$\rho_k(t) = r^k(t) + b_u(t) - b_s(t) + T(t) + \epsilon(t) \quad (4.13)$$

where r^k is the range to the satellite, b_u is the user clock bias, b_s is the satellite clock bias, T is the error caused by the troposphere, and ϵ is the unmodeled error. The range from the user to the satellite is calculated as

$$r^k = \|\mathbf{x}^k - \mathbf{x}_u\| \quad (4.14)$$

where \mathbf{x}^k is the three dimensional satellite position and \mathbf{x}_u is the three dimensional user position. The Newton-Raphson method is used to estimate the user position and user clock bias. An initial guess of user position is the same as 4.5. Next, the measurement matrix is formed

$$\hat{\rho} = \begin{bmatrix} -\frac{(\mathbf{x}_1 - \hat{\mathbf{x}}_u)}{\|\mathbf{x}_1 - \hat{\mathbf{x}}_u\|} + \hat{b} \\ -\frac{(\mathbf{x}_2 - \hat{\mathbf{x}}_u)}{\|\mathbf{x}_2 - \hat{\mathbf{x}}_u\|} + \hat{b} \\ \vdots \\ -\frac{(\mathbf{x}_n - \hat{\mathbf{x}}_u)}{\|\mathbf{x}_n - \hat{\mathbf{x}}_u\|} + \hat{b} \end{bmatrix} \quad (4.15)$$

The delta pseudorange is calculated as

$$\delta\rho = \rho - \hat{\rho} \quad (4.16)$$

The measurement matrix, H , is

$$H = \begin{bmatrix} (-\mathbf{1}^1) & 1 \\ (-\mathbf{1}^2) & 1 \\ \vdots & \vdots \\ (-\mathbf{1}^k) & 1 \end{bmatrix} \quad (4.17)$$

where $(\mathbf{1})$ is the unit vector of satellite position and user position.

The change in estimated position is calculated as

$$\begin{bmatrix} \delta\mathbf{x} \\ \delta b \end{bmatrix} = (G^T G)^{-1} G^T \delta\rho \quad (4.18)$$

The next iteration of user position estimate is calculated as

$$\hat{\mathbf{x}} = \mathbf{x}_0 + \delta\mathbf{x} \quad (4.19)$$

This process is solved iteratively until some threshold is met.

4.3 Testing Setup

The simulation is run through MATLAB as described at the beginning of this thesis. The settings are declared, the measurements are generated, the signal is created, and the signal is processed by a software receiver. An additional step may be included where the signal is passed through a universal software radio peripheral (USRP). The USRP demonstration is used to show that the signal generated in the simulation is capable of being passed through hardware. In this thesis an Ettus B200 mini USRP is used to perform a loopback function where the signal is played through the USRP and recorded by the same USRP. In order to do this, the generated signal cannot possess any errors. This is because the USRP will generate the errors on its own. The errors are background noise, transmitter clock error, and receiver clock error. The recorded signal is then passed through the software receiver for demodulation. This makes forming a position solution difficult and the results poor because the errors caused by the clock are unknown to the user.

To show the versatility of the simulation tool, the following tests have been conducted.

- Static receiver with no noise
- Static receiver played through USRP
- Static receiver with noise terms

- Static receiver with augmented satellites
- Dynamic receiver with no noise

Chapter 5

Results

This chapter will be used to show the results from simulations run in this thesis. The purpose of these results is to show that the simulation tool is capable of producing a signal that gives realistic results. Five tests will be performed; they are a static receiver with no signal noise and no measurement noise, a static receiver where the signal has been played through a USRP, a static receiver with noise terms added, a static receiver with no noise and augmented satellites, and a dynamic receiver with no noise.

While there are settings that will change between each simulation, some settings will remain constant. The sampling frequency of the measurements is 100Hz. Weather settings are set to 305.9 Kelvin, 85 percent humidity, and 1024 millibars of pressure. The mask angle is set to 1.7 degrees. The code frequency is 25,000 Hz. The signal sampling frequency is 1 MHz. the burst length is 20.32 milliseconds. The burst interval is 90 milliseconds. The data message used in the signal is the ECEF position and velocity vectors of the satellites.

Figures and metrics used to show results will include geo plots of estimated receiver positions, root mean square error, and position dilution of precision (PDOP). PDOP is a measure of how good the positions of the satellites are for positioning. More diversity between satellite positions will result in a lower PDOP. Low PDOP values indicate the diversity of satellites is good for positioning. GPS satellites typically have a PDOP value lower than 2 [4].

5.1 Static Clean Data

The data set generated for this scenario is a static data set with zero clock error, zero thermal signal noise, and zero atmospheric errors. The purpose of this experiment was to examine what

the cleanest possible data set would produce. The position of the receiver was placed in Auburn, Alabama with a location of [32.602236,-85.489192,201] in LLA. The simulation length is 15 minutes. The constellation used is the IridiumNext constellation.

For this data, the bit error rate of the decoded data is 99.07 percent for the in-phase branch and 99.087 percent for the quadrature branch.

5.1.1 Doppler Positioning

The first positioning strategy for this data set is using the received Doppler measurements in a batched fashion using the equations in section 4.1. Figure 5.1 shows the estimated receiver positions over the course of the simulation. The batch size for this was set at 2000 measurements. A few different batch sizes were used, however below 2000 measurements the positioning error was greater due to less measurements, and above 2000 measurements the solution change was minimal.

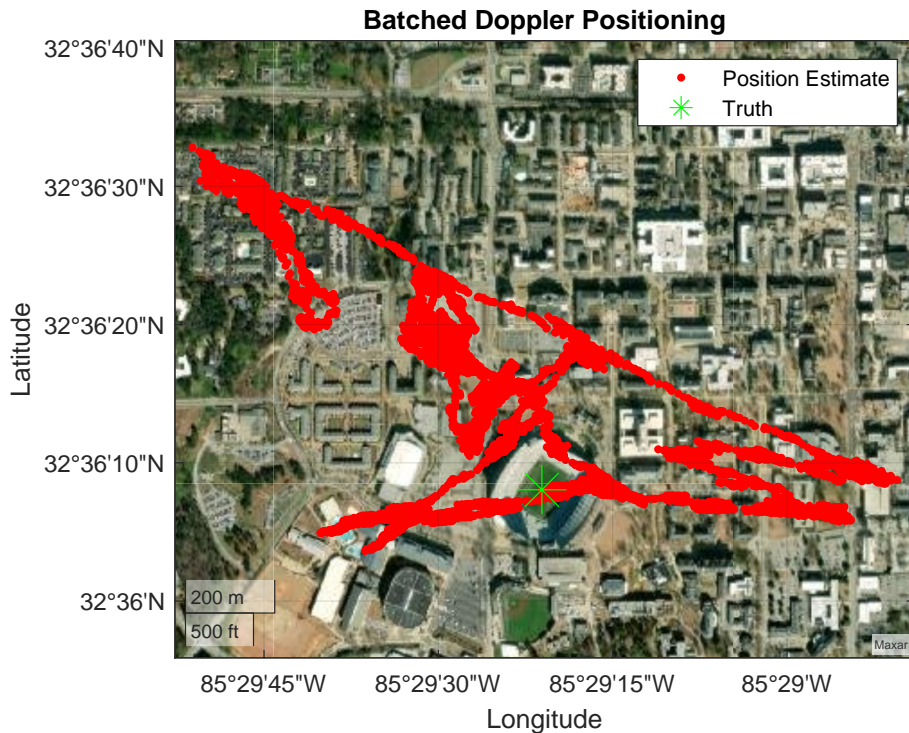


Figure 5.1: Position Estimate from Batched Doppler Measurements

The RMS positioning error is shown in Figure 5.2. The error in the Doppler positioning is caused by the error induced by the software receiver. In the software receiver, the Doppler

frequency is estimated to a degree of plus or minus 50 Hz. This combined with the satellite geometry and batching of measurements causes the error shown.

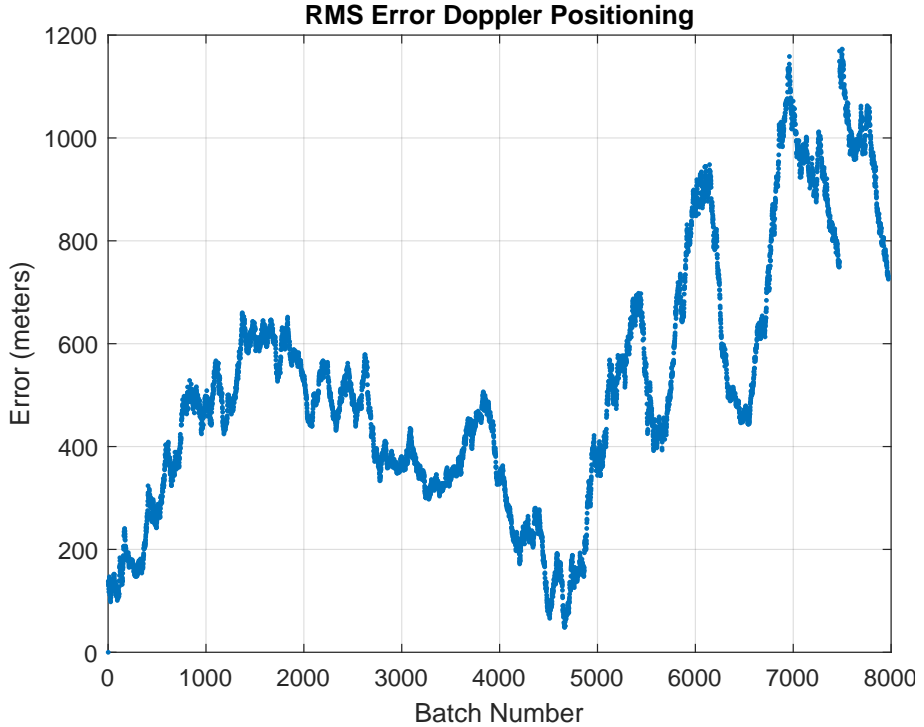


Figure 5.2: RMS Error of Batched Doppler Estimates

Figure 5.3 shows the PDOP from the batched Doppler measurements. This helps add reasoning to the poor positioning results of the batched doppler positioning. With values ranging from 29 to 52, the PDOP is significantly larger than what would be expected from GPS to give a good positioning solution.

5.1.2 Pseudorange Based Positioning

The next positioning strategy for this data set is using the calculated pseudorange measurements from 4.2. Figure 5.4 shows a geo plot of the estimated receiver position.

Figure 5.5 shows the root mean square error from truth of the estimated position. The positioning results from this are significantly better than the results from the Doppler positioning. In this technique, measurements are used from multiple satellites at different time points. A positioning solution is only calculated when there are a sufficient number of satellites with

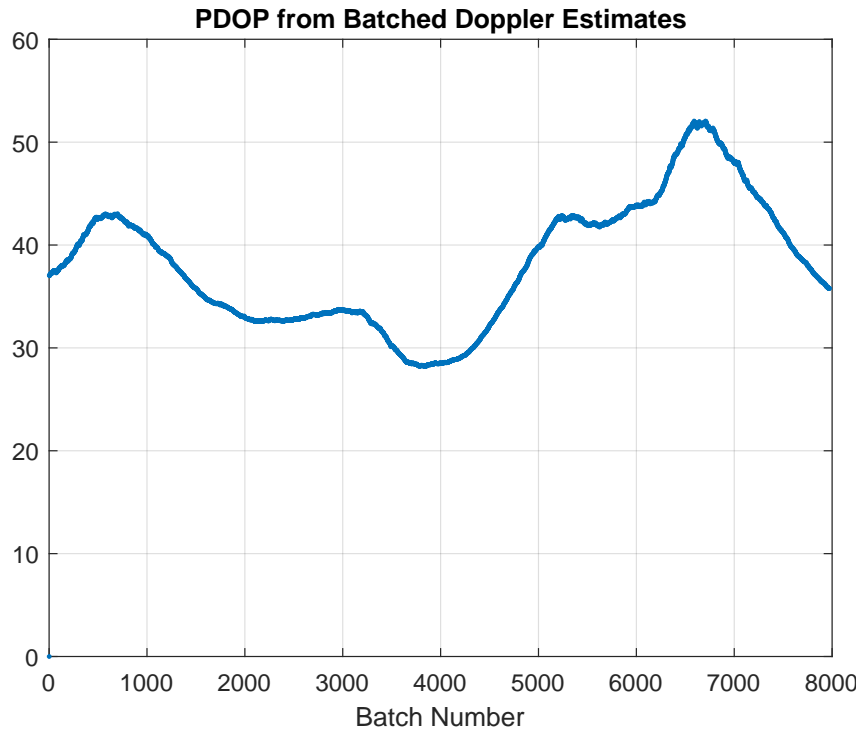


Figure 5.3: PDOP of Batched Doppler Estimates

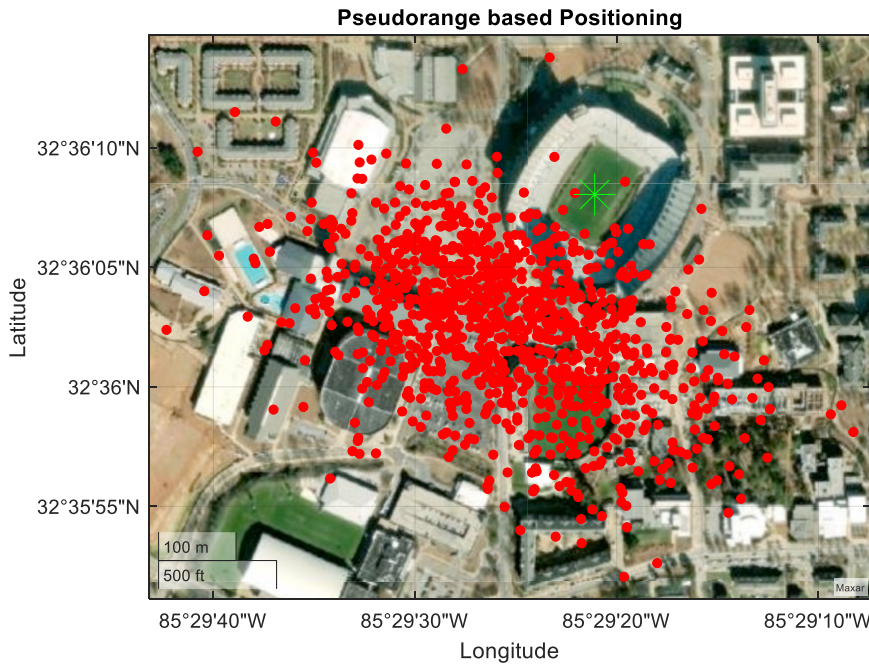


Figure 5.4: Position Estimate from Pseudoranges

unique measurements in view. In most GPS instances, the pseudorange positioning error is 10-15 meters [4]. In this instance, the positioning is not as accurate. This could be due to the lower sampling frequency used for this simulation. The resolution of the pseudorange measurements

is lowered due to the lower sampling frequency. If the sampling frequency was higher, more change in bit location could be detected.

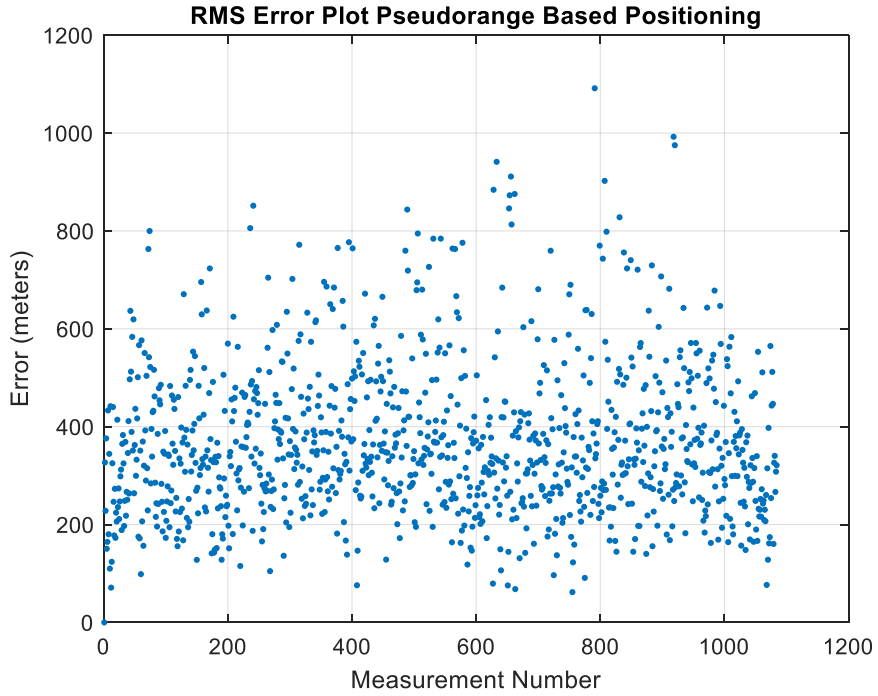


Figure 5.5: RMS Error from Pseudoranges

Figure 5.6 shows the PDOP. The PDOP for this simulation is also significantly better than that of the Doppler positioning PDOP and stays around a typical value that would be seen in GPS pseudorange positioning techniques.

5.2 Static Clean Data Played Through USRP

For this simulation, everything from the previous simulation remains the same. The only difference between the two tests is before the signal is passed through the software receiver, it is played through a USRP. The USRP used is the B200 mini from Ettus Research. The USRP will add thermal background noise, transmitter and receiver clock error, and other unmodeled errors. These errors will contribute to poor positioning results as the errors cannot all be estimated with the algorithms used in this thesis. If the transmitter clock error was known, the receiver clock error could be estimated and vice versa. However the algorithm cannot estimate both errors simultaneously. In order to gain a positioning solution, satellite navigation data was

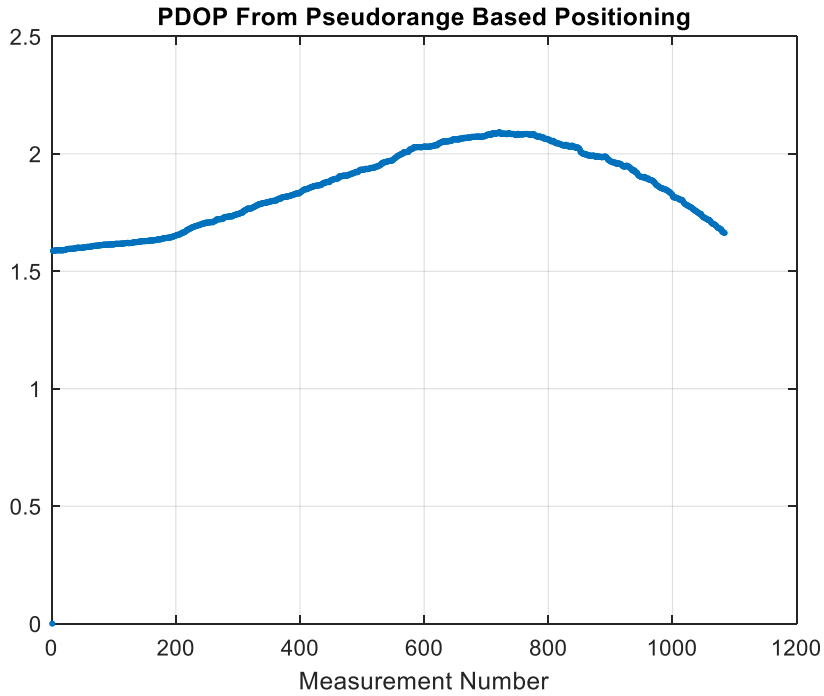


Figure 5.6: PDOP from Pseudoranges

filtered to remove outliers in satellite positions and velocities. In this simulation, 9,435 bursts were decoded and 506 bursts were not decoded properly resulting in 94.91 percent decoded. The quadrature bit error rate is 98.0448 percent, and the in-phase bit error rate is 97.8867 percent.

5.2.1 Doppler Positioning

The Doppler positioning geo plot is shown in Figure 5.7. Initially, the positioning results are not terrible, however at batch number 175, the solution begins to grow unbounded. Once the initial guess goes off track, the algorithm cannot correct for the large offset. The estimated position grows due to errors in the decoded satellite navigation message. Even after the error detection the solution grows to infinity. Since the next position estimate is initialized with the previous estimate, the position estimate will become increasingly worse. After batch number 275 the solution grows to infinity and the rest of the estimates cannot be computed.

Figure 5.8 shows the error seen in Figure 5.7. Again, it can be seen that the error grows around batch number 170 and then returns closer to truth after batch number 250. It would have been expected to see 8000 batched positioning solutions, however less than 300 were computed.

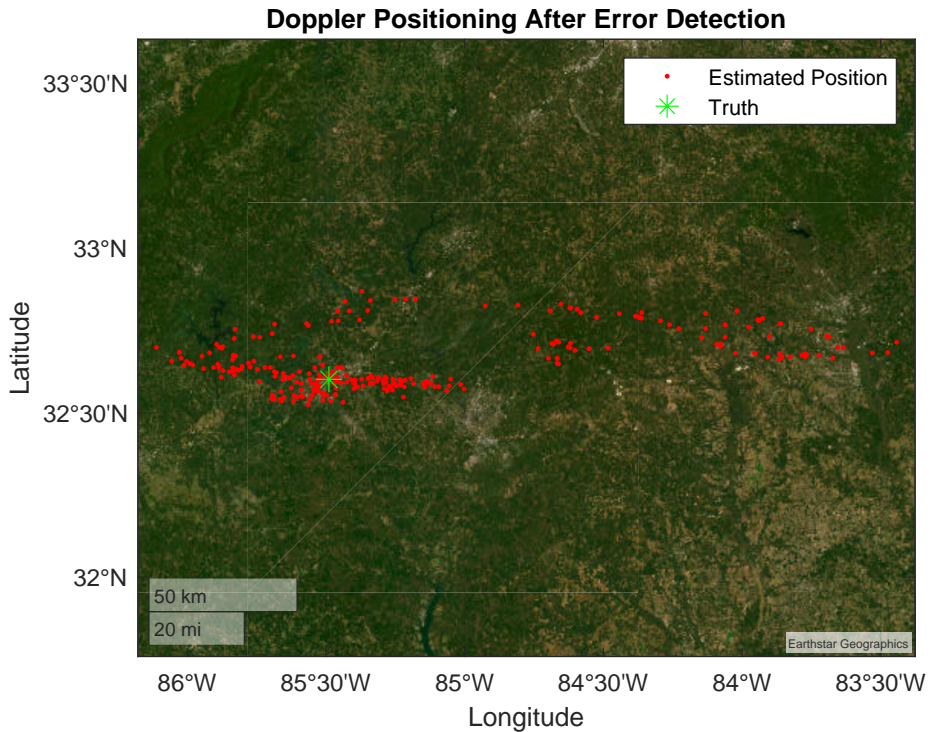


Figure 5.7: USRP Doppler Positioning Estimate

This because once the diverts from a value near truth, the solution grows unbounded towards infinity.

Figure 5.9 shows that at the begining of the simulation, the PDOP is poor. The PDOP remains around 3000 until near the end where it begins to decrease, however the measurement errors cause the estimate to grow unbounded and no more estimates to be calculated.

5.2.2 Pseudorange Based Positioning

Figure 5.10 gives the geo plot of the pseudorange based positioning estimates. The pseudorange based positioning is better, but is still significantly poor when compared to the case with no noise. The position can be seen drifting across the geo plot. This may be caused by the clock error in the USRP. Figure 5.11 shows that the majority of the position estimates remain low, however there are still some outlier position estimates. Other possible errors could be caused by bit errors caused by the USRP. This would cause the change in bit location to have error contributing to noisy pseudorange measurements.

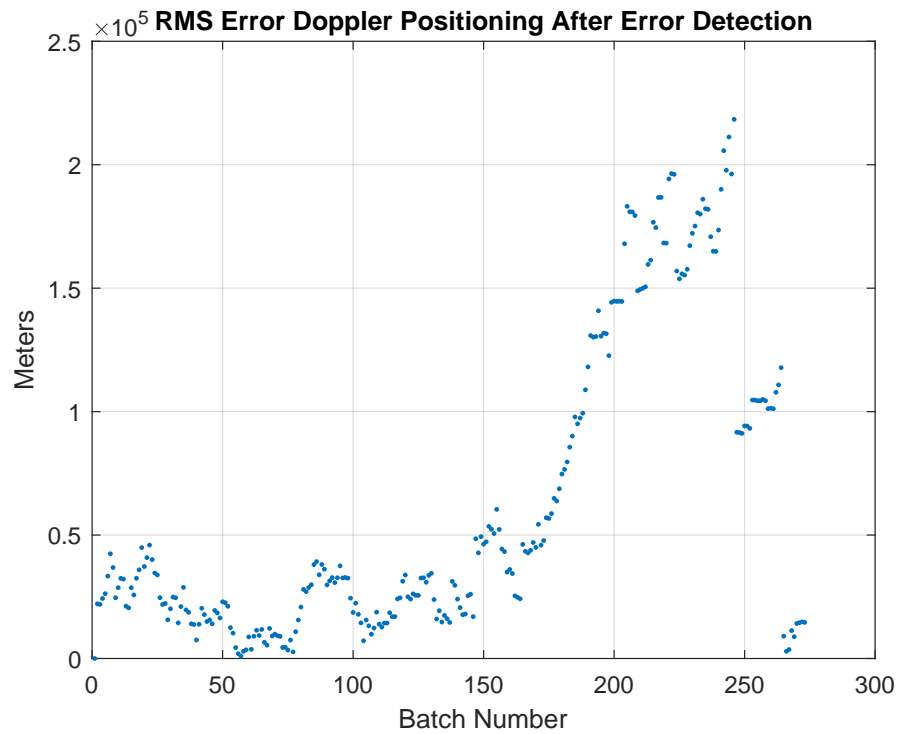


Figure 5.8: RMS Error of Doppler Positioning Estimate

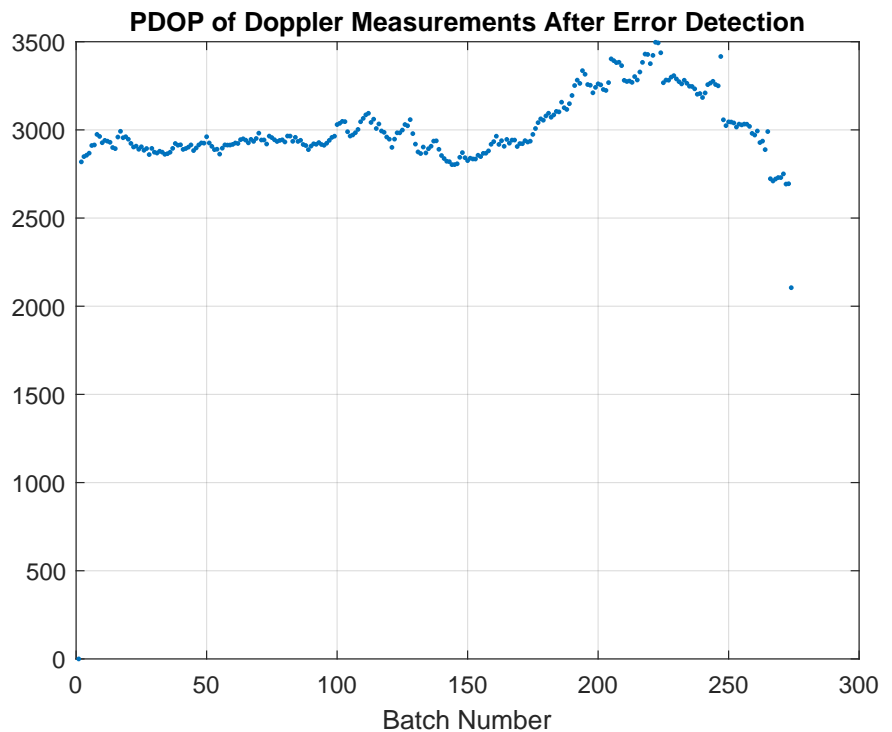


Figure 5.9: PDOP from Doppler Positioning Estimate

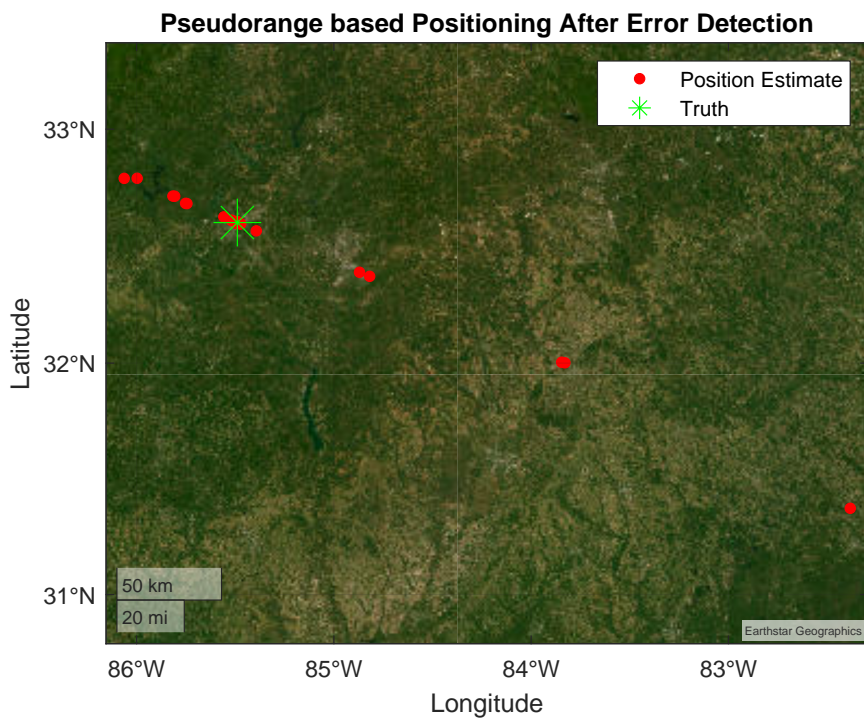


Figure 5.10: USRP Pseudorange Positioning Estimate

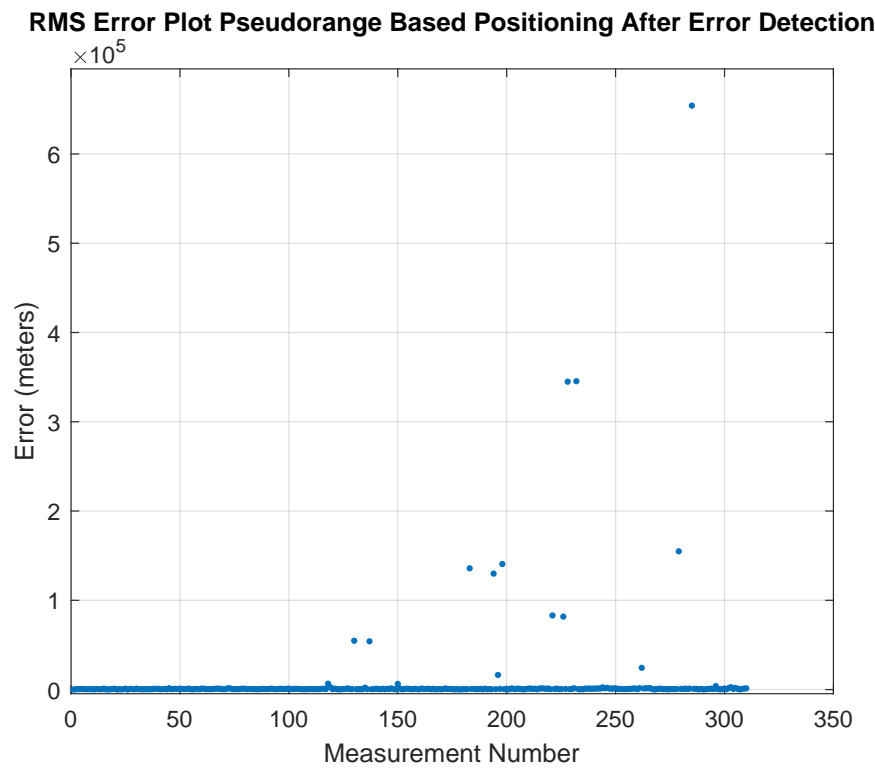


Figure 5.11: RMS Error USRP Pseudorange Positioning Estimate

Figure 5.12 shows the PDOP from the pseudorange based positioning estimate. The PDOP is significantly better than the PDOP from the Doppler based positioning. However instead of being a smooth curve as expected, there are outliers along the curve that match the same position as the larger positioning errors.

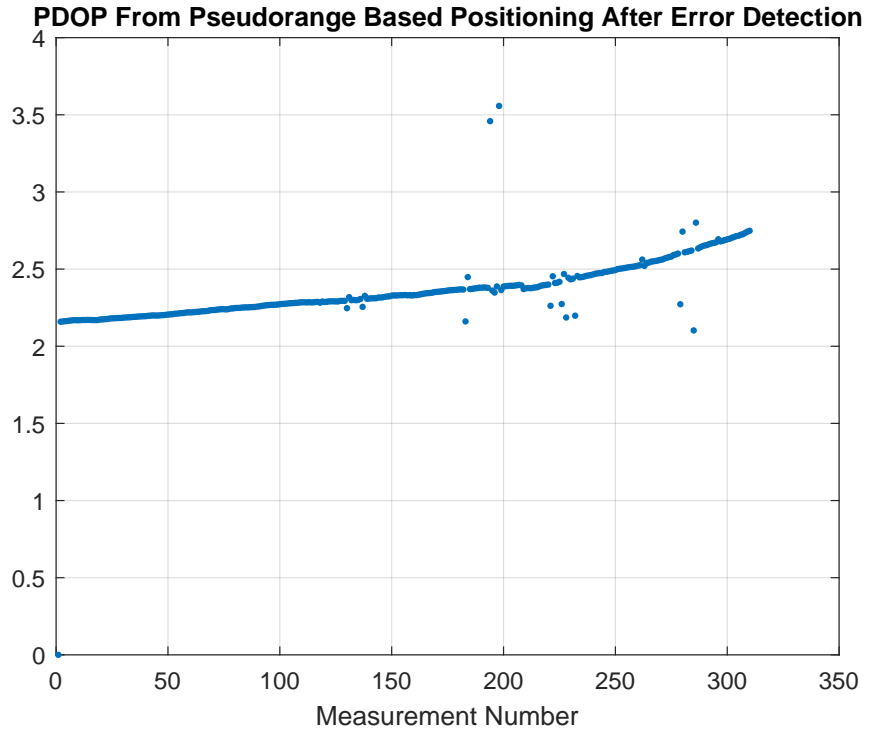


Figure 5.12: USRP Pseudorange Positioning Estimate PDOP

5.3 Static Noisy Data

In this section, a simulated signal with signal noise and measurement noise is generated. The user clock was modeled as an OCXO. The satellite clock error is simulated as zero for simplicity. This is because the error caused by the satellite clock would be transmitted and immediately be removed from the measurement. The carrier to noise ratio for the signal is set to 65. The quadrature bit rate error is 98.5423 percent and the in-phase bit rate error is 99.1743 percent.

5.3.1 Doppler Positioning

The Doppler positioning of this data set is shown in Figure 5.13. This solution is better than the estimates provided from the USRP data set. The batch size used for this position estimate is 2000 measurements.

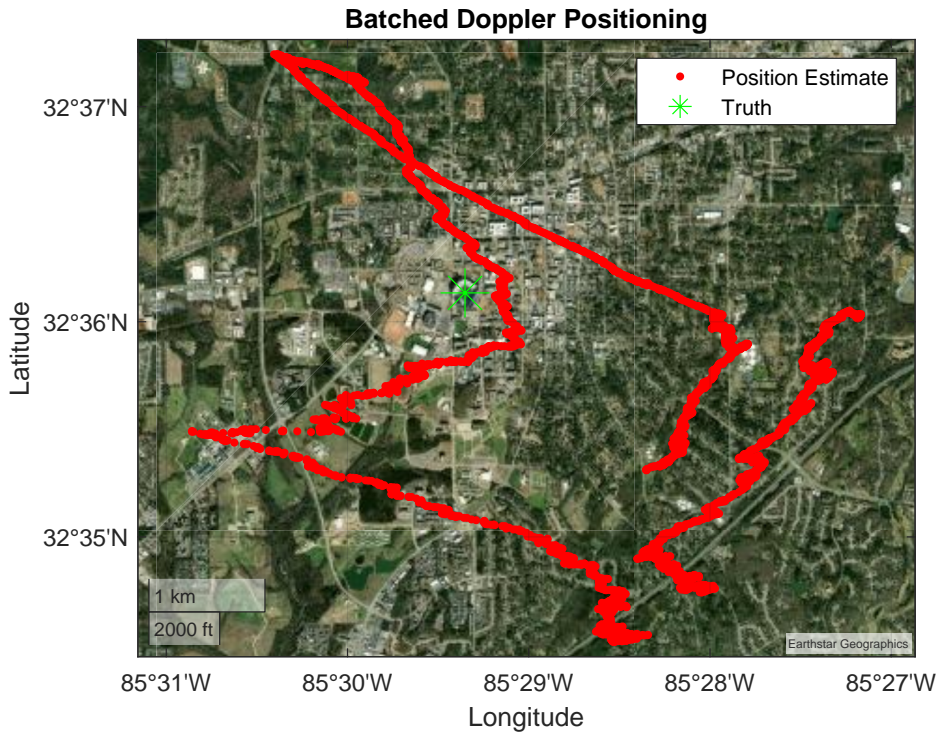


Figure 5.13: Noisy Doppler Positioning Estimate

Figure 5.14 shows the RMS error from truth. The closest estimate is near 1000 meters with a maximum error around 4250 meters. These errors can be attributed to the error caused by the received Doppler estimates and the clock drift. While the clock drift is estimated by the receiver, batching the estimates causes error. This is because the clock drift is averaged across all the measurements over time instead of instantaneously. For example, if the batch number is 2000 and the burst time is 0.09s, there are 180 seconds where the drift grows.

Figure 5.15 shows the PDOP across the batches. The spike in error around batch number 3000 could be attributed to the spike in PDOP. At this point, the diversity in satellites is lower and most of the measurements are coming from one satellite instead of multiple. The drop in

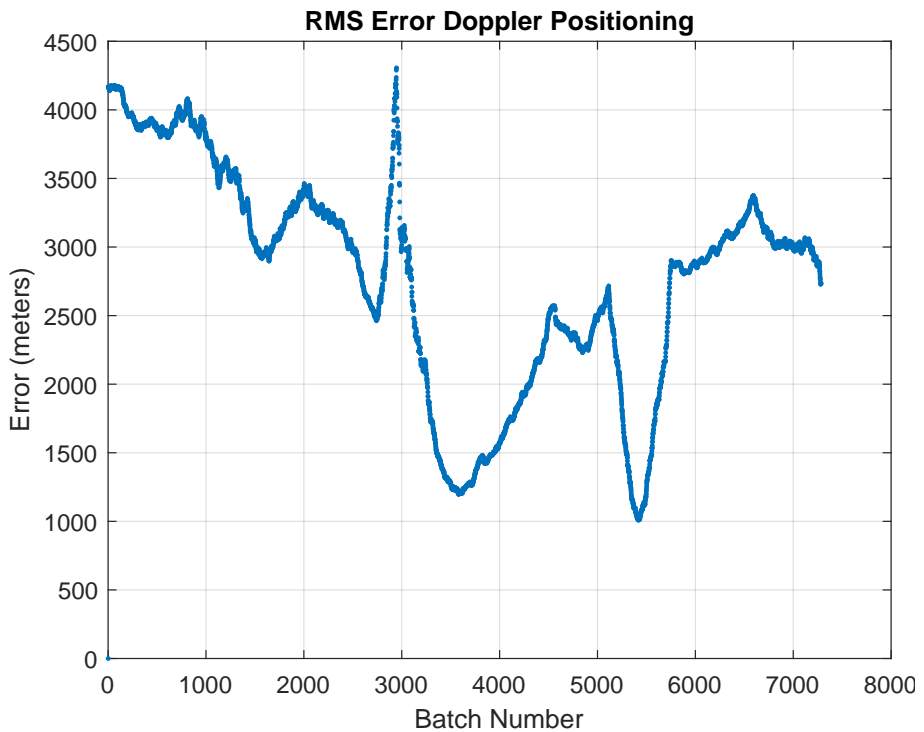


Figure 5.14: RMS Error Noisy Doppler Positioning Estimate

PDOP is where an additional satellite comes into view and there is more diversity in the satellite measurements.

5.3.2 Pseudorange Based Positioning

Figure 5.16 shows the geo plot of the pseudorange based positioning. In this example, the pseudorange has Tropospheric noise, clock bias, and additional un-modeled effects with a mean of 5 meters of error. This figure shows receiver estimate when the errors have not been taken out of the measurement. The error is worse than the Doppler based positioning. Figure 5.17 shows the distribution RMS error of the pseudorange based positioning. At its highest, the error is nearly 30 kilometers, where the lowest is within 100 meters.

The PDOP in Figure 5.18 is the highest of all the simulations. It starts near 57 and eventually trails off to 22.

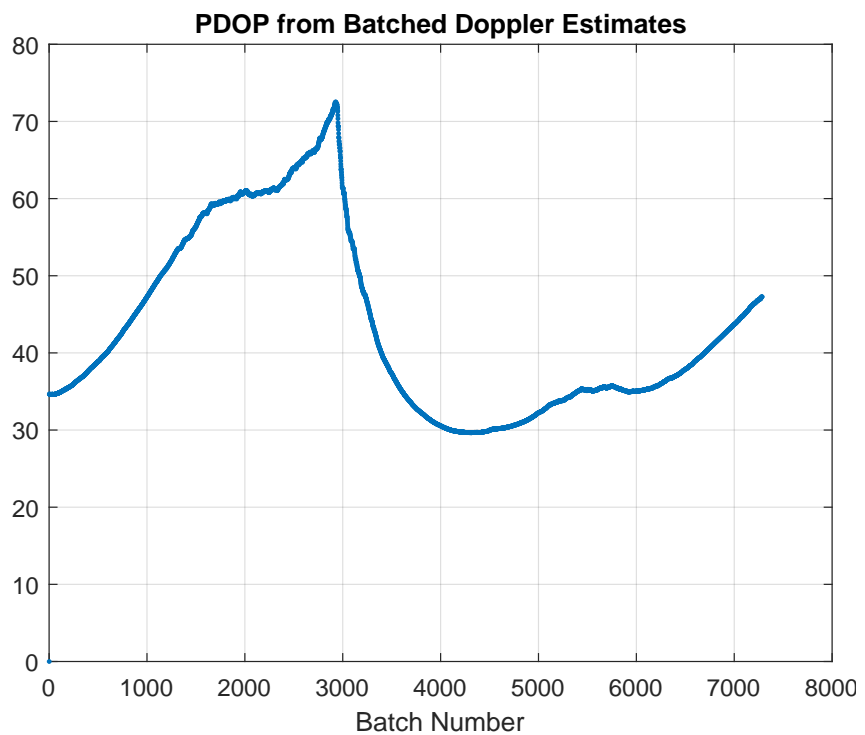


Figure 5.15: Noisy Doppler Positioning PDOP

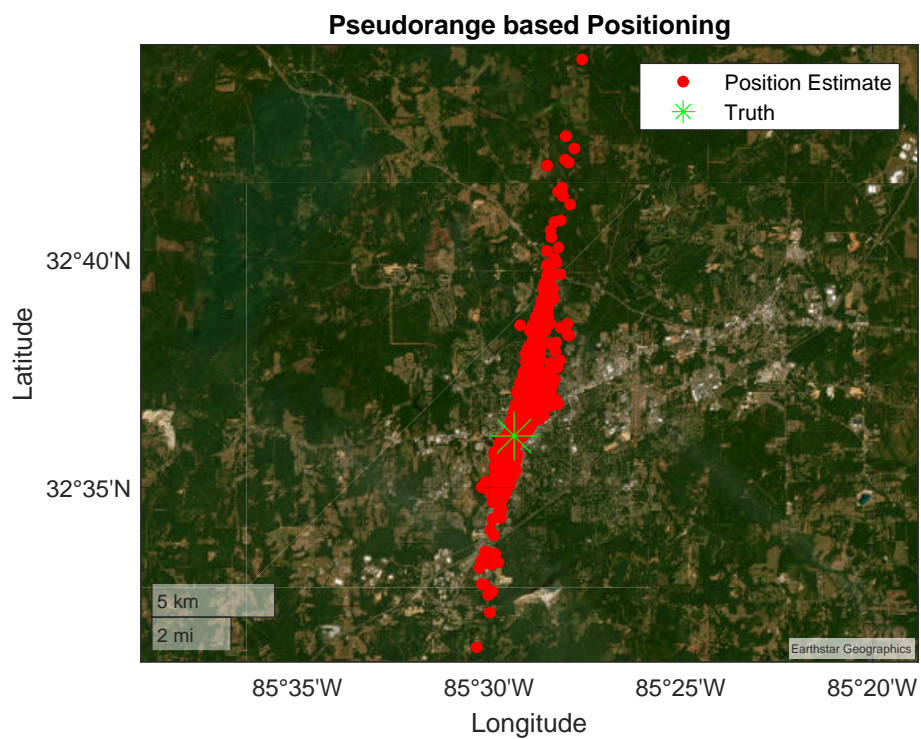


Figure 5.16: Noisy Pseudorange Positioning Estimate

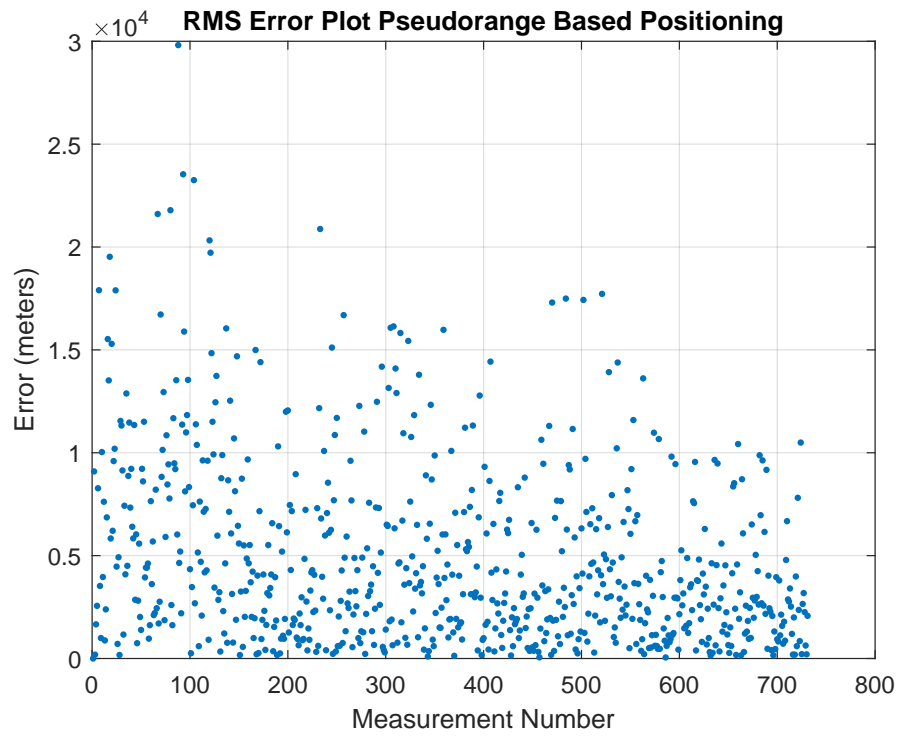


Figure 5.17: RMS Error Noisy Pseudorange Positioning Estimate

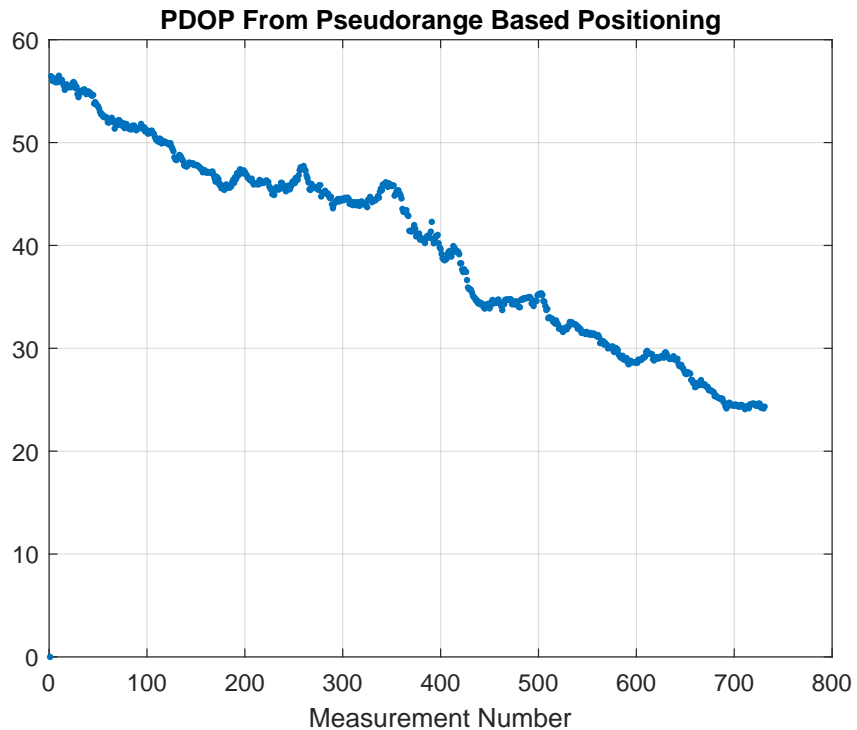


Figure 5.18: PDOP Dirty Pseudorange Positioning Estimate

5.4 Static Augmented Satellites

To show the versatility of the simulation tool, a simulation of augmented satellites was performed. In this simulation, the simulation length is 5 minutes. The main satellite constellation is the IridiumNext constellation. All noise terms are turned off. The augmented constellation has 8 orbital planes, 15 satellites per plane, an inclination angle of 45 degrees, and an orbit altitude of 800 kilometers. The receiver is placed at the 50 yard line of Jordan-Hare Stadium in Auburn, Alabama [32.602236,-85.489192,201]. The bit error rate for both the in-phase and quadrature are 99.9624 percent. Figure 5.19 shows the orbit paths of the IridiumNext constellation augmented with additional satellites.

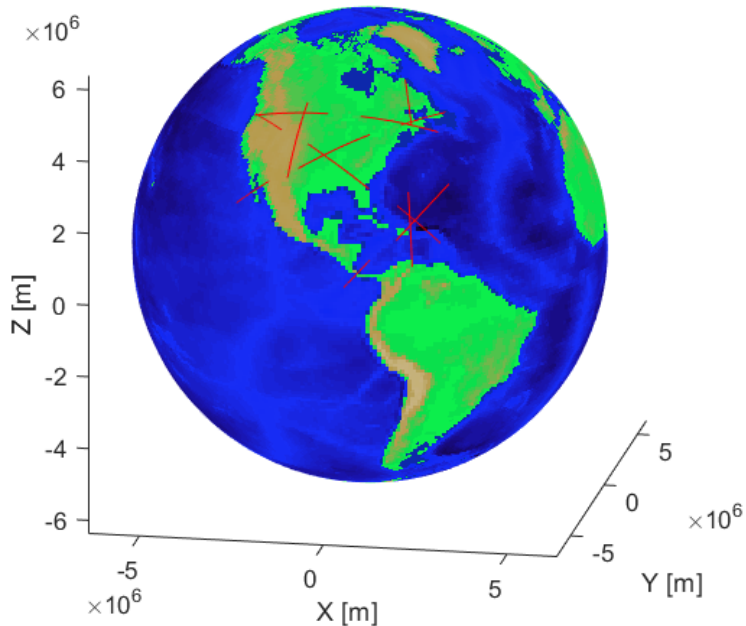


Figure 5.19: Generated Augmented Satellite Constellation

Figure 5.20 shows the skyplot of the augmented satellites over the period of the simulation.

5.4.1 Doppler Positioning

The same Doppler positioning technique is used for this example. Figure 5.21 shows the estimated receiver positions. It can be seen that the grouping of receiver estimates seems to be

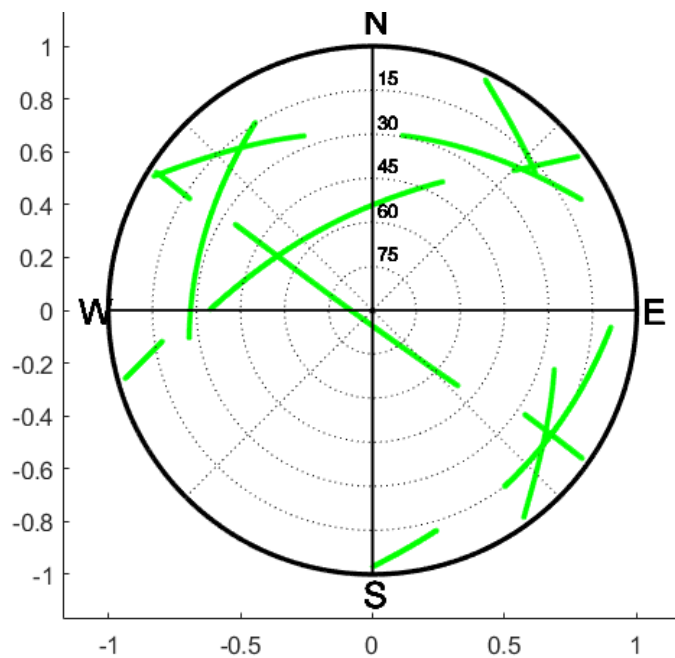


Figure 5.20: Skyplot of Augmented Constellation

biased by around 1000 meters. One possible reason for this is that the satellite positions do not favor the southwest area of the sky.

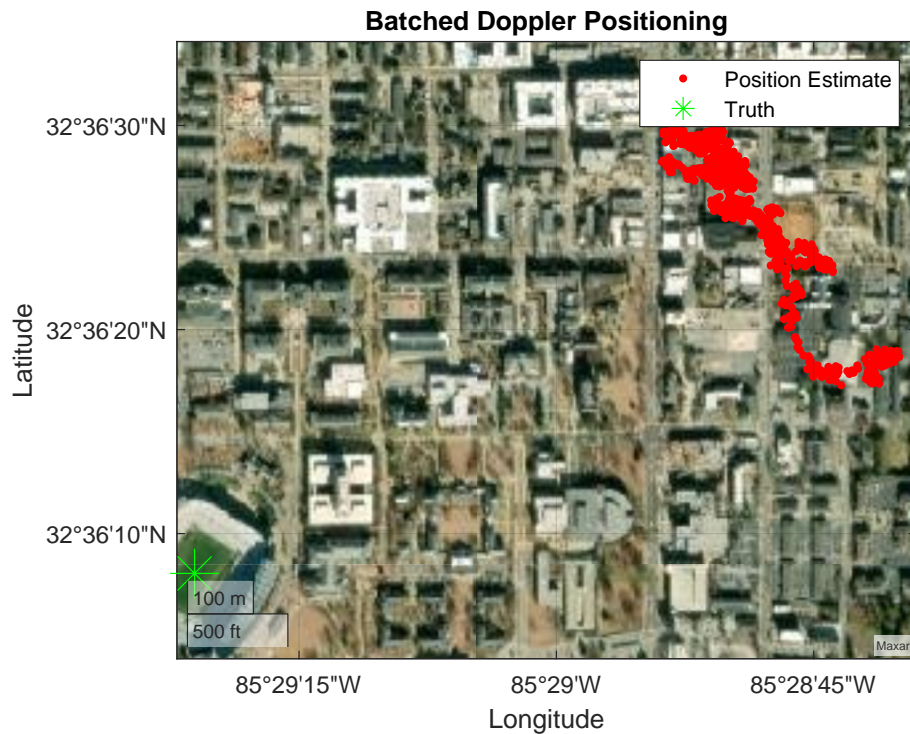


Figure 5.21: Doppler Position Estimates of Augmented Satellites

The constant bias can be seen in Figure 5.22. The positioning error is most likely caused by the error induced by the software receiver. Figure 5.23 shows the PDOP of each batched

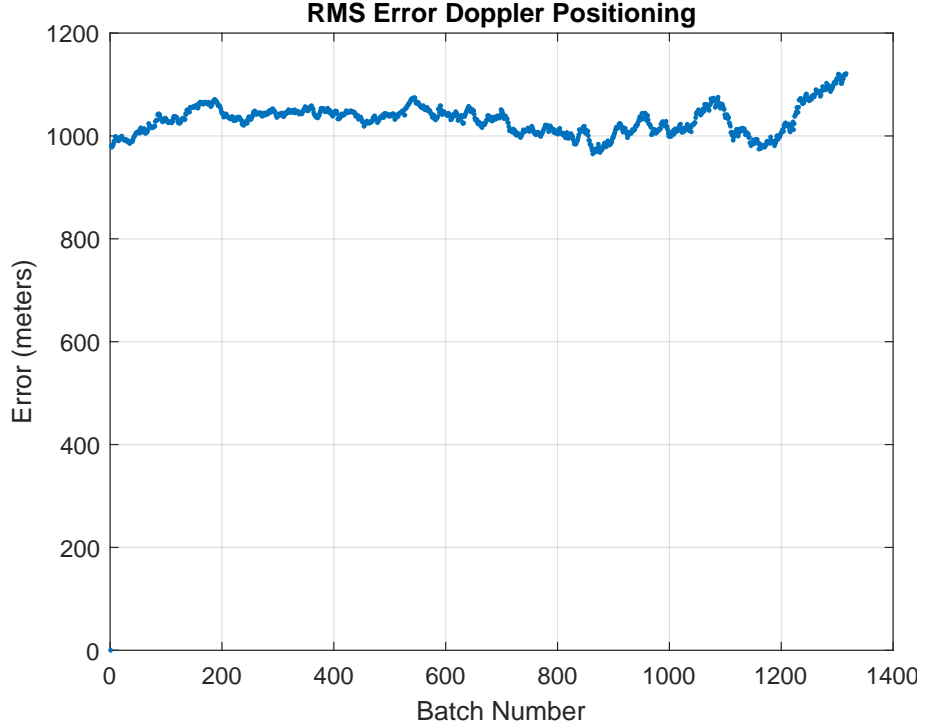


Figure 5.22: RMS Error Doppler Position Estimates of Augmented Satellites

measurement. With the addition of more satellites, the PDOP fluctuates less and is the best of all simulations shown in this thesis. By adding more diversity to the satellites, the PDOP improves. While this is still not a GPS quality PDOP, it is more stable than the PDOP of the IridiumNext constellation.

5.4.2 Pseudorange Based Positioning

The pseudorange based positioning estimates are shown in Figure 5.24. While there are more position estimates in the Doppler solution, the RMS error is better in the pseudorange solution. The RMS error is shown in 5.25. The error is lower than in any of the previous simulations. The error in the pseudorange is most likely caused by the low resolution caused by the low sampling frequency.

Figure 5.26 shows that the increased number of satellites has improved the PDOP from the IridiumNext simulation. Overall, the increased number of satellites has improved the position-

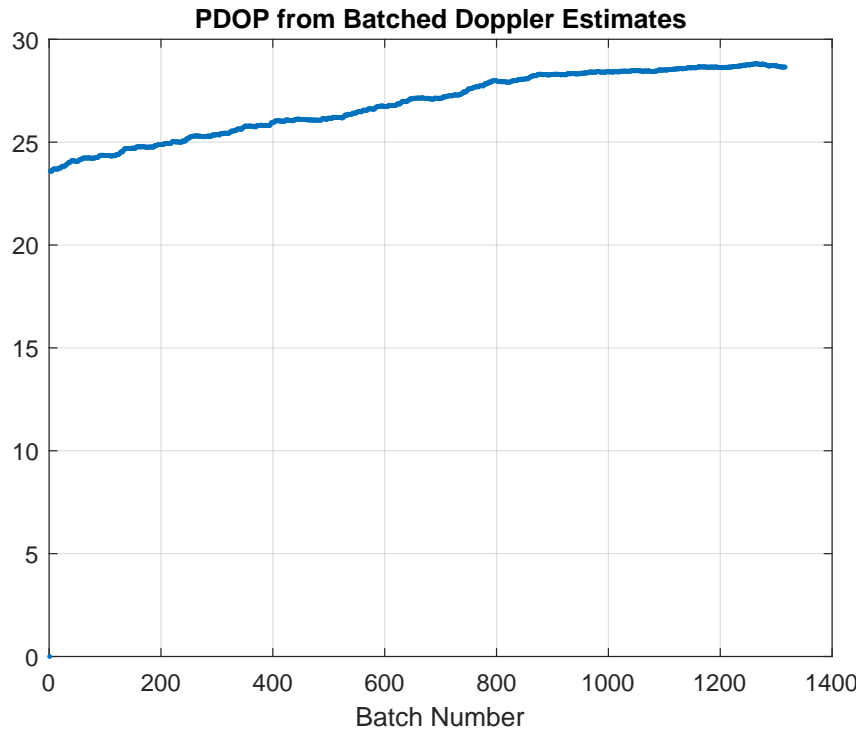


Figure 5.23: PDOP of Doppler Position Estimates of Augmented Satellites

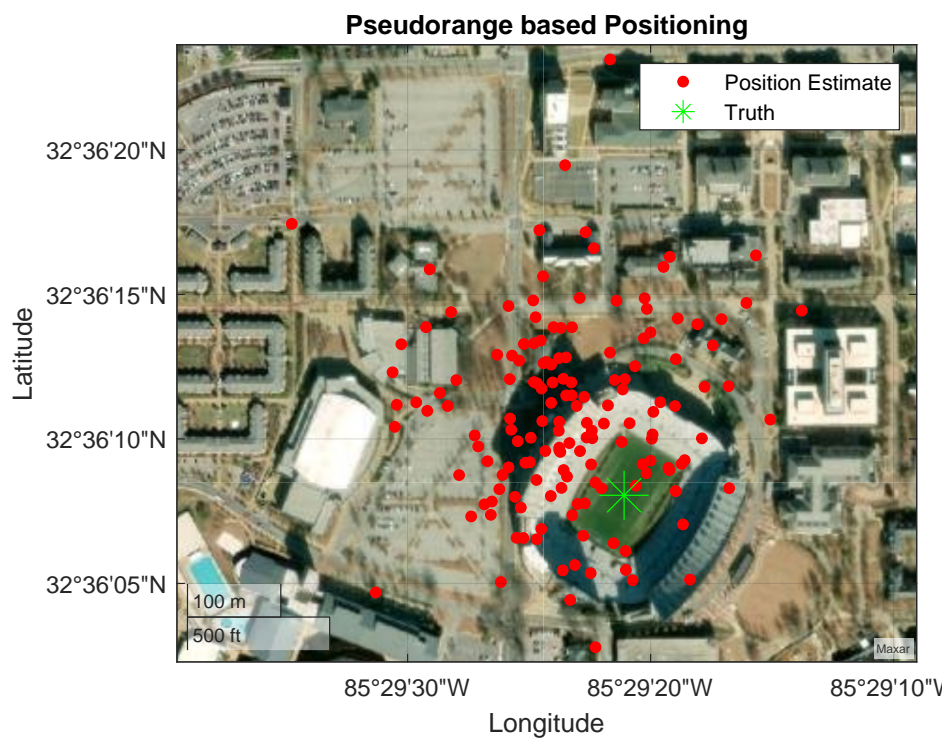


Figure 5.24: Pseudorange Position Estimates of Augmented Satellites

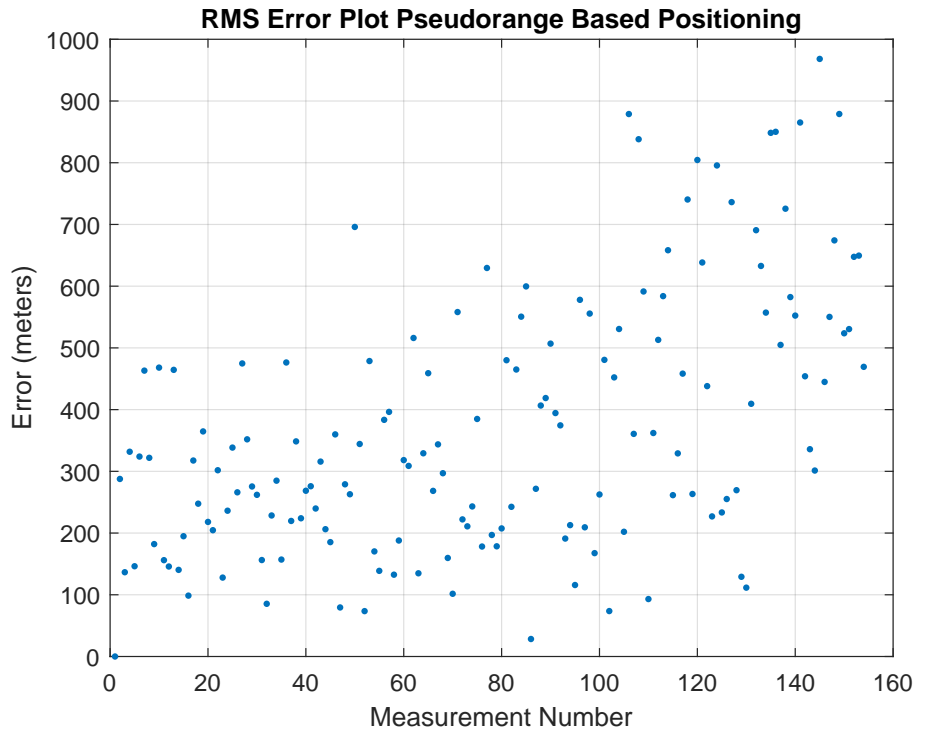


Figure 5.25: RMS Error of Pseudorange Position Estimates of Augmented Satellites

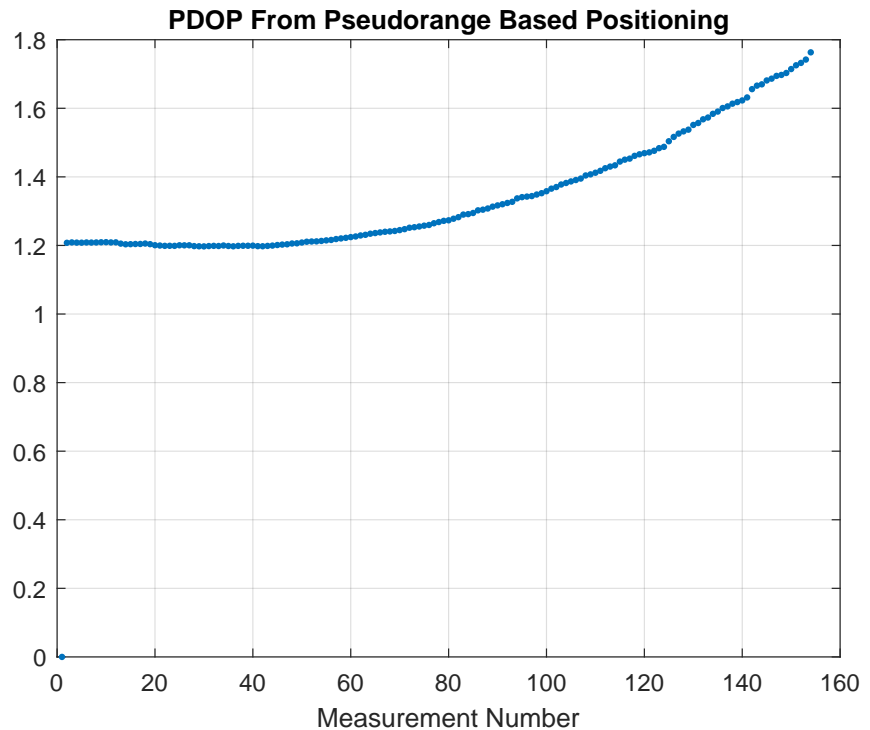


Figure 5.26: PDOP of Pseudorange Position Estimates of Augmented Satellites

ing estimate. This is expected as more satellites result in an increased number of measurements and an increased diversity of satellite locations.

5.5 Dynamic Clean Data

Another capability of this simulator is the ability to generate data for dynamic trajectories. For a dynamic trajectory simulation, the user will begin by setting the user position and velocity to a predetermined path. The position and velocity will be in the ECEF coordinate frame. The data set used for this test was taken by driving a path with a Lincoln MKZ that had an eTalin measurement device. A plot of the path driven is shown below in Figure 5.27

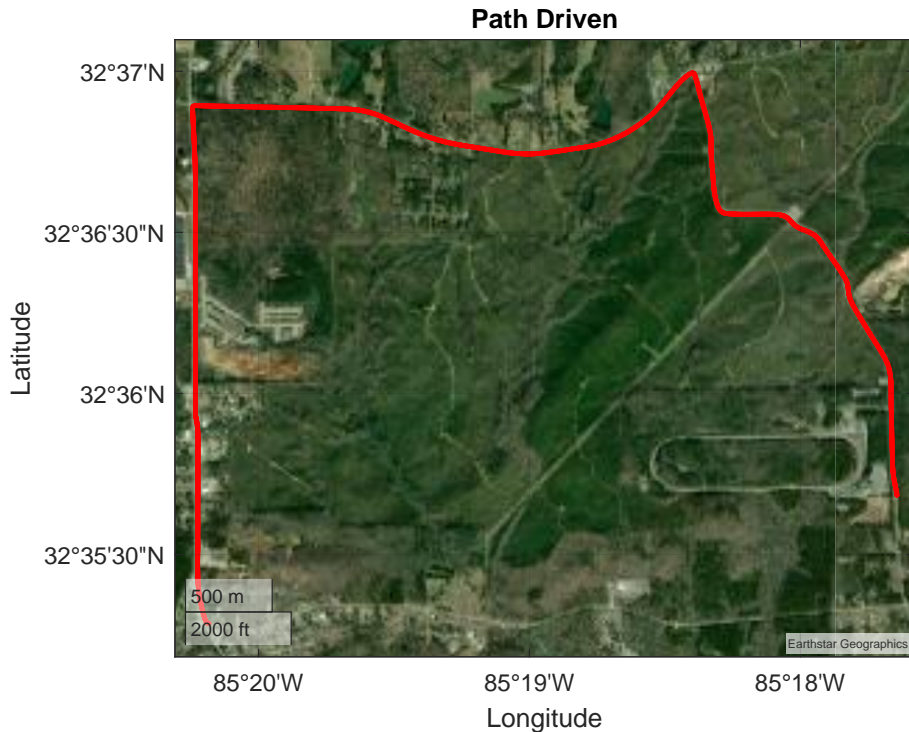


Figure 5.27: Path Driven for Dynamic Data

The positioning techniques used in this thesis are not applicable to dynamic positioning because they are for a static receiver and require batched measurements to calculate a position. A positioning solution will not be calculated for the dynamic test. To show an output of the simulation, the received Doppler frequency of the generated signal will be compared against Doppler measurements from a Jackson Labs receiver. The Jackson Labs receiver is an Iridium specific receiver for the satellite timing and location (STL) signal. Figure 5.28 shows the

generated Doppler frequencies for the dynamic test. Figure 5.29 shows the live sky received Doppler frequencies from the Jackson Labs receiver.

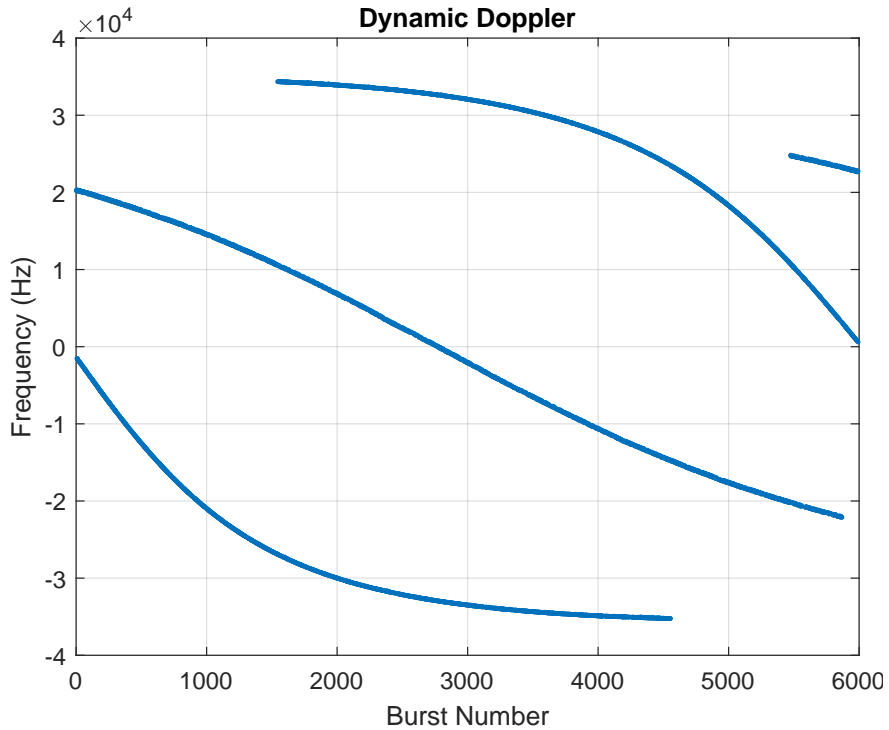


Figure 5.28: Generated Dynamic Doppler Measurements

It was important to sync the simulation time with the actual time of the data run to accurately simulate the satellites that were in view at the time of the data collection. Even with syncing up the time of simulation to the data collection, the simulated satellite positions were not accurate to the live sky data. Also, the assumption in this simulation tool is that the receiver will receive a burst at each interval, however in the real world this is not the case. There is also a larger mask angle from satellites in the real world due to buildings, trees, and landscape. This decreases the number of bursts received by the receiver.

The purpose of this experiment was to prove that a signal could be calculated for a dynamic data set. While the receiver position could not be estimated, the output and comparison of Doppler frequencies shows that the simulator is capable of generating a signal for a dynamic trajectory and successfully receive the data.

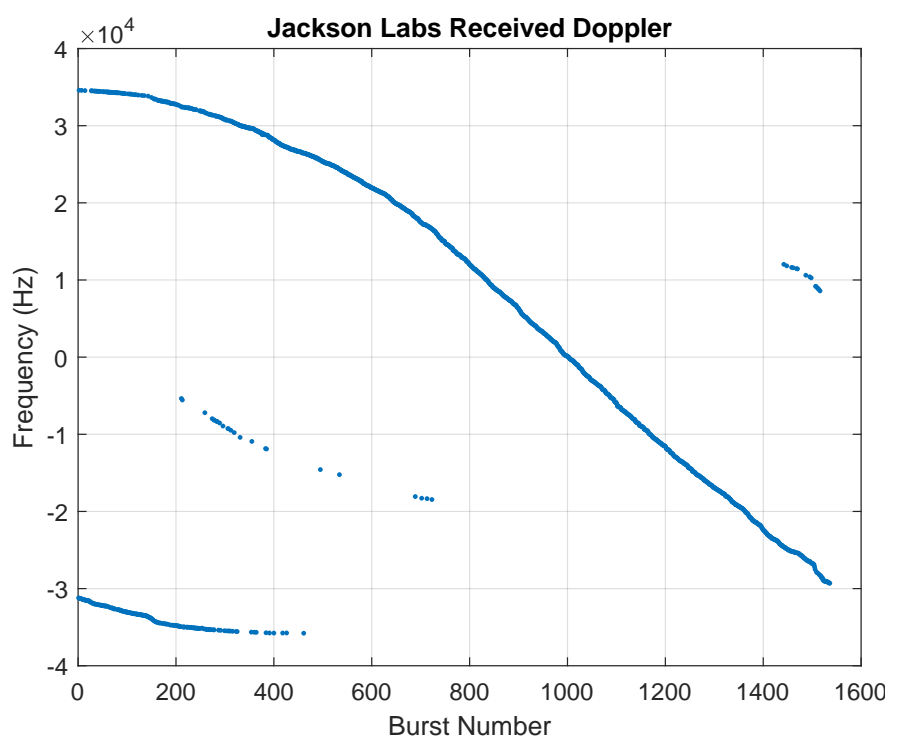


Figure 5.29: Jackson Labs Doppler Measurements

Chapter 6

Conclusions and Future Work

6.1 Summary

Chapter 1 discusses the motivation behind this thesis and why there is a need for a LEO satellite signal simulation tool. Having a simulation tool to test current and hypothetical signals and satellite constellations for investigative purposes is important in the engineering process. Before hardware is developed or satellites are launched, the constellation and signals need to be tested in software. Testing in software allows for changes to be made in the development process where the cost of changes are minimal. Once satellites are launched and hardware has been assembled, the margin to change is thin. Simulation tools allow for fast testing and validation of techniques and algorithms. This simulation in particular aids the engineering process by being able to generate signals for satellite constellations that can be processed through software receivers with the possibility of hardware receivers. This chapter also discusses prior work with LEO satellites and GNSS signal simulators. Most of the prior work is aimed at using LEO satellites as signals of opportunity to aid navigation solutions in areas of poor GNSS reception. This is followed by the contributions of this thesis and an outline.

Chapter 2 begins with a brief introduction to satellite based navigation where the trilateration is introduced. This is followed by describing different orbit zones around the Earth and what satellites occupy that specific space. Next channel access methods such as TDMA, CDMA, and FDMA are mentioned in brief. Chapter 2 is concluded by mentioning different modulation techniques.

Chapter 3 discusses the simulation tool in parts. It begins by giving an overview of the entire simulation process. Next the simulation settings are defined along with all of the terms the user can change. The measurement simulation is discussed fully where the inputs and outputs are explained and what their purpose is later in the simulation. The mathematical calculation of measurements are also given in this section. The process of generating the signal is discussed. Finally, the receiver used in this thesis is described.

Chapter 4 defines the testing setup and positioning techniques. In this thesis, multiple different simulations were conducted to show the versatility of the tool. The testing setup is mainly in software, but there is the introduction of a USRP to show the generated signal has the ability to be played into hardware. The positioning techniques used in this thesis are a batched Doppler least squares estimate and a pseudorange least squares estimate.

Chapter 5 provides the positioning results of the output signal data. Geographical plots of the position estimates, RMS error, and PDOP are used to show how the outputs of the signal are used. This is the validation that the generated signal could be used for navigation and that the generated signal is real.

6.2 Conclusions

This thesis developed a simulation tool capable of generating navigation signals for LEO satellites. The simulation tool works well for its purpose. It has shown the ability to generate realistic IQ data for LEO satellites. The ability to test different constellation configurations, signal types, data messages, error types, and other settings is vital to a simulation tool worth being used. This thesis has accomplished making contributions in the field of navigation. A comprehensive simulation tool for generating measurements and signals for LEO satellites was developed. The signal showed that it could be played through a software receiver and a USRP. Positioning techniques for a TDMA signal were used to validate the signal. While the positioning results are not as robust as a standard GNSS positioning solution, the navigation data was proven to provide a positioning solution.

6.3 Future Work

The future work for this project can take the direction of making additions to the simulation tool. The addition of multiple signal types would be beneficial as new and emerging satellite constellations will need to be simulated. A modular software receiver tied directly to the signal simulation would make the process of receiving the signal more streamline. The addition of more error terms, such as ionospheric error would improve the quality of the simulation tool. Another addition could be the addition of a clock model that more accurately describes the nature of clocks used in satellites and receivers. With new emerging satellite constellations such as Starlink and Xona, the addition of those satellite constellations and signals could be an avenue to pursue.

More future work could include developing a hardware receiver for a specific receiver to test the capability of this simulation tool. It could be interesting to see how this signal simulation would work with a hardware in the loop (HWIL) simulation. For an HWIL project, a predetermined signal type and data message structure would need to be decided before work on the hardware could begin. Once the signal had been decided upon, the user could begin rearranging the simulation tool to match the desired signal.

A futher expansion of this thesis is to develope a more rigorous navigation message. While the navigation message in this thesis works, the introduction of a higher fidelity satellite propagation model will require more terms to account for corrections. Also, the addition of more positioning techniques as forms of colaborative navigation could be interesting to investigate.

Bibliography

- [1] Amplitude Shift Keying.
- [2] Frequency Shift Keying.
- [3] Ghafour Amouzad Mahdiraji and Ahmad Fauzi Abas. Advanced Modulation Formats and Multiplexing Techniques for Optical Telecommunication Systems. March 2010.
- [4] Pratap Misra and Per Enge. *Global Positioning System; Signals, Measurements, and Performance*. Ganga-Jamuna Press, Lincoln, Massachusetts, revised second edition edition, 2012.
- [5] Lei Dong. *IF GPS Signal Simulator Development and Verification*. PhD thesis, University of Calgary, Alberta, Calgary, Canada, November 2003.
- [6] Phillip Martin Corbell. *Design and Validation of an Accurate GPS Signal and Receiver Truth Model for Comparing Advanced receiver Processing Techniques*. PhD thesis, Air Force Institute of Technology, Wright-Patterson Air Force Base, Ohio, March 2000.
- [7] Russell Powell. *A Multiple-Antenna Software GPS Signal Simulator forRapid Testing of Interference Mitigation Techniques*. PhD thesis.
- [8] Wu-Hung Hsu and Shau-Shiun Jan. Assessment of using Doppler shift of LEO satellites to aid GPS positioning. In *2014 IEEE/ION Position, Location and Navigation Symposium - PLANS 2014*, pages 1155–1161, Monterey, CA, USA, May 2014. IEEE.
- [9] Mark L. Psiaki. Navigation using carrier Doppler shift from a LEO constellation: TRAN-SIT on steroids. *NAVIGATION*, 68(3):621–641, September 2021.

- [10] Mojtaba Bahrami. GNSS Doppler Positioning (An Overview). page 17.
- [11] Transit Satellite: Space-based Navigation.
- [12] Sterling Thompson. Single Differenced Doppler Positioning with Low Earth Orbit Signals of Opportunity and Angle of Arival Estimation. In *Proceedings of the 2021 International Technical Meeting*, pages 497–509, Long Beach, CA, January 2021.
- [13] Remy Lopez, Jean-Pierre Malarde, Francois Royer, and Philippe Gaspar. Improving Argos Doppler Location Using Multiple-Model Kalman Filtering. *IEEE Transactions on Geoscience and Remote Sensing*, 52(8):4744–4755, August 2014.
- [14] Joe J. Khalife and Zaher M. Kassas. Receiver Design for Doppler Positioning with Leo Satellites. In *ICASSP 2019 - 2019 IEEE International Conference on Acoustics, Speech and Signal Processing (ICASSP)*, pages 5506–5510, May 2019. ISSN: 2379-190X.
- [15] Zizhong Tan, Honglei Qin, Li Cong, and Chao Zhao. New Method for Positioning Using IRIDIUM Satellite Signals of Opportunity. *IEEE Access*, PP:1–1, June 2019.
- [16] Joshua J. Morales, Joe Khalife, Ali A. Abdallah, Christian T. Ardito, and Zak M. Kassas. Inertial Navigation System Aiding with Orbcomm LEO Satellite Doppler Measurements. pages 2718–2725, Miami, Florida, October 2018.
- [17] Tyler G.R. Reid, Bryan Chan, Ashish Goel, Kazuma Gunning, Brian Manning, Jerami Martin, Andrew Neish, Adrien Perkins, and Paul Tarantino. Satellite Navigation for the Age of Autonomy. In *2020 IEEE/ION Position, Location and Navigation Symposium (PLANS)*, pages 342–352, April 2020. ISSN: 2153-3598.
- [18] NOAA US Department of Commerce. Satellites. Publisher: NOAA’s National Weather Service.
- [19] Rob Garner. GOES Overview and History, March 2015.
- [20] GLONASS Interface Control Document. page 47, 1998.

- [21] Mohamad Orabi, Joe Khalife, and Zak Kassas. Opportunistic Navigation with Doppler Measurements from Iridium Next and Orbcomm LEO Satellites. April 2021.
- [22] Iridium NEXT: In Review, February 2019.
- [23] Starlink.
- [24] R. Gold. Optimal binary sequences for spread spectrum multiplexing (Corresp.). *IEEE Transactions on Information Theory*, 13(4):619–621, October 1967. Conference Name: IEEE Transactions on Information Theory.
- [25] GLONASS Signal Plan - Navipedia.
- [26] R.G. Brown and P.Y.C Hwang. *Introduction to Random Signals and Applied Kalman Filtering*. John Wiley and Sons, fourth edition, February 2012.
- [27] Howard D. Curtis. *Orbital mechanics for engineering students*. Elsevier Aerospace engineering series. Elsevier Butterworth Heinemann, Amsterdam Heidelberg, 1. ed., reprinted edition, 2008.
- [28] E.H. Dinan and B. Jabbari. Spreading codes for direct sequence CDMA and wideband CDMA cellular networks. *IEEE Communications Magazine*, 36(9):48–54, September 1998. Conference Name: IEEE Communications Magazine.
- [29] Samuel McDougal, Samuel Morgan, and Scott Martin. Single-Antenna Low Earth Orbit Signal Simulator for Hardware in the Loop Testing. In *35th International Technical Meeting of the Satellite Division of the Institute of Navigation (ION GNSS+ 2022*, pages 2349–2361, Denver, CO, September 2022.

Appendices